1 **Engineering and Evolution of Methanol Assimilation in *Saccharomyces***

2 ***cerevisiae***

3 Monica I. Espinosa [1,2], Ricardo A. Gonzalez-Garcia [3], Kaspar Valgepea [3,4], Manuel Plan [3,5],

4 Colin Scott [2,6], Isak S. Pretorius [1], Esteban Marcellin [3,5], Ian T. Paulsen [1]* and Thomas C.

5 Williams [1,2]*

6 [1] ARC Centre of Excellence in Synthetic Biology, Department of Molecular Sciences, Macquarie University, NSW,

7 Australia

8 [2] CSIRO Synthetic Biology Future Science Platform, Canberra, ACT 2601, Australia

9 [3] Australian Institute for Bioengineering and Nanotechnology, The University of Queensland, St. Lucia, Australia

10 [4] ERA Chair in Gas Fermentation Technologies, Institute of Technology, University of Tartu, Tartu, Estonia

11 [5] Metabolomics Australia, AIBN, The University of Queensland, Brisbane, Australia

12 [6] Biocatalysis and Synthetic Biology Team, CSIRO, Canberra, Australia

13

14 * Corresponding authors: tom.williams@mq.edu.au, ian.paulsen@mq.edu.au

15

Abstract

17 Microbial fermentation for chemical production is becoming more broadly adopted as an

18 alternative to petrochemical refining. Fermentation typically relies on sugar as a feedstock,

19 however, one-carbon compounds like methanol are an attractive alternative as they can be

20 derived from organic waste and natural gas. This study focused on engineering methanol

21 assimilation in the yeast *Saccharomyces cerevisiae*. Three methanol assimilation pathways were

22 engineered and tested: a synthetic xylulose monophosphate (XuMP), a 'hybrid' methanol

23 dehydrogenase-XuMP, and a bacterial ribulose monophosphate (RuMP) pathway, with the latter

24 identified as the most effective at assimilating methanol. Additionally, ^{13}C-methanol tracer

25 analysis uncovered a native capacity for methanol assimilation in *S. cerevisiae*, which was

26 optimized using Adaptive Laboratory Evolution. Three independent lineages selected in liquid

27 methanol-yeast extract medium evolved premature stop codons in *YGR067C*, which encodes an

28 uncharacterised protein that has a predicted DNA-binding domain with homology to

29   the *ADR1* transcriptional regulator. Adr1p regulates genes involved in ethanol metabolism and

30   peroxisomal proliferation, suggesting *YGR067C* has a related function. When one of the

31   evolved *YGR067C* mutations was reverse engineered into the parental CEN.PK113-5D strain,

32   there were up to 5-fold increases in ^{13}C-labelling of intracellular metabolites from ^{13}C-labelled

33   methanol when 0.1 % yeast extract was a co-substrate, and a 44 % increase in final biomass.

34   Transcriptomics and proteomics revealed that the reconstructed *YGR067C* mutation results in

35   down-regulation of genes in the TCA cycle, glyoxylate cycle, and gluconeogenesis, which

36   would normally be up-regulated during growth on a non-fermentable carbon source. Combining

37   the synthetic RuMP and XuMP pathways with the reconstructed Ygr067cp truncation led to

38   further improvements in growth. These results identify a latent methylotrophic metabolism in *S.*

39   *cerevisiae* and pave the way for further development of native and synthetic one-carbon

40   assimilation pathways in this model eukaryote.

Introduction

Our current dependence on fossil fuels is not sustainable due to their finite reserves and the negative environmental impacts caused by their use. By-products from fossil fuel combustion include a myriad of toxic air pollutants and CO_2, which is the main anthropogenic contributor to climate change. These complex environmental problems call for a global effort to move towards a bio-economy in which microbial metabolism is used for the conversion of renewable materials into useful products [1]. Typically, sugars derived from sugarcane or corn are used as feedstocks for the production of fuels and chemicals using biological fermentation. However, sugar production is costly and requires arable land that competes with other land uses, such as food production. It is estimated that the sugar cost represents up to 70 % of the total production costs [2], making many biotechnological processes uncompetitive with petrochemical processes.

Growing crops for feedstock also requires water and fertilizer, which could be instead allocated to grow food to meet the demand of an ever-rising population. Alternatively, lignocellulosic non-food biomass could be used for obtaining sugars, but the process is limited by the recalcitrance of the feedstock and difficulties utilising the large lignin fraction of biomass. One-carbon (C1) metabolites are abundant and inexpensive, and can be obtained from natural gas or waste resources such as agricultural, municipal or industrial waste, or natural gas [3,4]. Methanol in-particular is becoming an attractive feedstock due to its abundance and liquid state, which makes it more compatible with existing fermentation, storage, and transportation infrastructure [3,5]. Methanol can also be obtained inexpensively from methane and carbon dioxide stemming from industrial waste streams [6]. Engineering microorganisms to grow on and convert C1 compounds such as methanol into food, fuels, and chemicals has therefore become a major goal in the fields of synthetic biology and metabolic engineering [7,8].

Methylotrophic metabolism enables energy and biomass generation from methanol, and is present in bacterial, archaeal, and yeast species. Recent attempts have been made to produce

68   valuable metabolites using methylotrophs. For example, *Methylobacterium extorquens* AM1

69   has been engineered to produce 3-hydroxypropionic acid from methanol [9]. The methylotrophic

70   yeast *Pichia pastoris* (renamed *Komagataella phaffii* [10]) is currently used industrially for

71   production of recombinant proteins [11]. Recently, *P. pastoris* has also been used for production

72   of metabolites including astaxanthin and isobutanol [12,13]. However, relative to model organisms,

73   native methylotrophs lack the genetic tools and depth of characterisation necessary for the

74   successful metabolic engineering of high-yield and heterologous pathways. An attractive

75   alternative to enable the use of methanol as feedstock is to engineer synthetic methylotrophy

76   into industrially-robust and well-characterised microorganisms. Model organisms are not only

77   easier to genetically manipulate and optimise, but also provide the opportunity to engineer non-

78   native central carbon metabolism that has greater genetic and metabolic plasticity. Recent

79   approaches have focused on engineering synthetic methylotrophy in bacteria such as

80   *Escherichia coli* and *Corynebacterium glutamicum* [14-21]. Incorporation of ^{13}C-methanol into

81   central carbon metabolites and specialty products has been demonstrated in both species;

82   however, growth on methanol still requires yeast extract or additional carbon sources like

83   xylose.

84

85   The yeast *Saccharomyces cerevisiae* has potential as a host for the engineering of synthetic

86   methylotrophy as it has distinct advantages over organisms such as *E. coli* for use in industrial

87   fermentation. For example, *S. cerevisiae* can correctly express, fold, and post-translationally

88   modify eukaryotic proteins, is not susceptible to phage contamination, has high tolerance to low

89   pH concentrations and solvents like methanol, and has organelles that can be co-opted for

90   localization of specialized metabolism [22-24]. The engineering of synthetic methylotrophic

91   metabolism in *S. cerevisiae* could therefore provide several benefits for methanol-fed

92   bioprocesses. Here, we designed, built, and tested three different methanol-assimilation

93   pathways in *S. cerevisiae* and identified for the first time the native capacity of *S. cerevisiae* to

94   assimilate methanol into central carbon metabolism. Using methanol-dependent growth assays,

95   ^{13}C-methanol tracer studies, and Adaptive Laboratory Evolution (ALE), we characterised

96 synthetic methanol assimilation pathways and optimised native methanol assimilation in *S.*
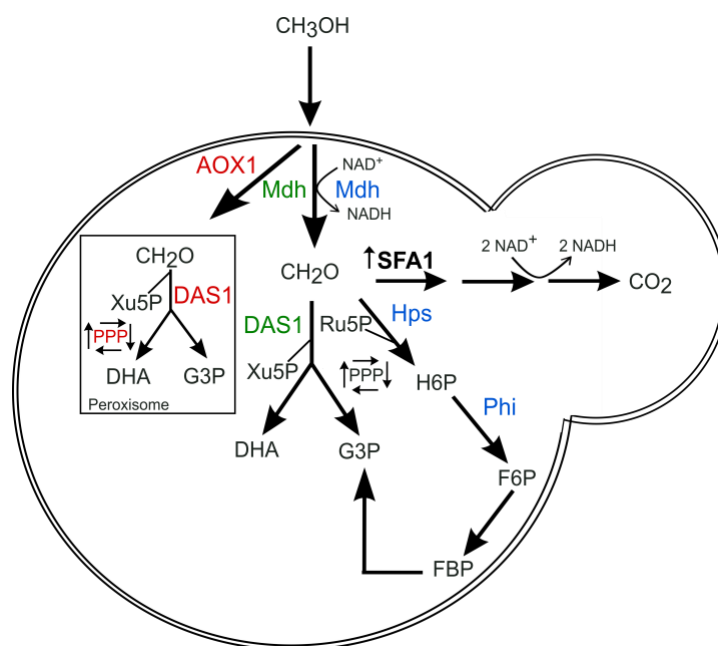
97 *cerevisiae*.

98

99 **Results**

100 **Benchmarking synthetic pathways for methanol assimilation potential**

101 After evaluating the different methanol assimilation pathways that have been previously

102 described in nature, three metabolic pathways were designed for engineering synthetic

103 methylotrophy in *S. cerevisiae*. The first pathway design (coloured red in Fig. 1A) was based on

104 the xylulose monophosphate (XuMP) pathway in the methylotrophic yeast *P. pastoris*. Here,

105 methanol assimilation genes are targeted to the peroxisome by a type 1 peroxisome targeting

106 signal (PTS1). An FAD-dependent alcohol oxidase (Aox1p) oxidises methanol to formaldehyde

107 and hydrogen peroxide. Hydrogen peroxide is detoxified by a catalase (Cat1p) in the

108 peroxisome while formaldehyde is converted to glyceraldehyde-3-phosphate by

109 dihydroxyacetone synthase (Das1p), which uses xylulose-5-phosphate as a co-substrate.

110 Glyceraldehyde-3-phosphate can then be incorporated into central carbon metabolism to

111 produce biomass. The second pathway was termed a 'hybrid' because it links the *P. pastoris*

112 XuMP pathway with an NAD_+-dependent methanol dehydrogenase (Mdh) from *Bacillus*

113 *stearothermophilus*, which oxidises methanol to formaldehyde but does not produce hydrogen

114 peroxide. Formaldehyde is then converted to glyceraldehyde-3-phosphate by a cytosolically

115 localised Das1p from *P. pastoris*. Utilising Mdh has the advantage of not requiring oxygen for

116 the reaction and not producing hydrogen peroxide, unlike Aox1p, and generating energy in the

117 form of NADH. The third pathway was based on the bacterial ribulose monophosphate (RuMP)

118 pathway where Mdh oxidises methanol to formaldehyde while hexulose-6-phosphate synthase

119 (Hps) uses ribulose-5-phosphate as a co-substrate to convert formaldehyde to hexulose-6-

120 phosphate, which is then converted to fructose-6-phosphate by 6-phospho-3-hexuloisomerase

121 (Phi) from *Bacillus methanolicus*. Fructose-6-phosphate can then enter glycolysis to produce

122 biomass precursors.

123   The three pathways, yeast XuMP, 'hybrid' XuMP, and bacterial RuMP, were expressed from

124   low-copy centromeric plasmids in *S. cerevisiae* and tested by spotting serial 10-fold dilutions of

125   the strains onto solid minimal Yeast Nitrogen Base (YNB) medium with 1 %, 2 %, or 4 %

126   methanol alongside an empty vector control (CEN.PK113-5D; Fig. 1B). These spot assays are a

127   high-throughput method for assaying growth, with colony size and spot-density comparisons

128   used to identify growth differences. To determine if the growth differences were methanol-

129   specific, strains were also spotted onto solid minimal YNB medium with 2 % glucose, YNB

130   medium with no added carbon source (1 x YNB) or 2 % methanol with 0.1 % yeast extract (Fig.

131   1B). The yeast XuMP pathway (*P. pastoris AOX1* and *DAS1*) resulted in a subtle growth

132   increase on 1 % methanol medium compared to the empty vector control, but this was not

133   visible at 2 % methanol. The 'hybrid' XuMP pathway with bacterial *mdh* and *P. pastoris DAS1*

134   expression had increased growth on 1 % and 2 % methanol relative to the control strain. The

135   same was observed in the bacterial RuMP pathway with *mdh*, *hps*, and *phi*. Growth was still

136   observed on 1 x YNB medium with no added carbon source, indicating there are medium

137   components that enable the observed background growth. Strain-specific growth differences

138   were far more pronounced on YNB-methanol media without yeast-extract.
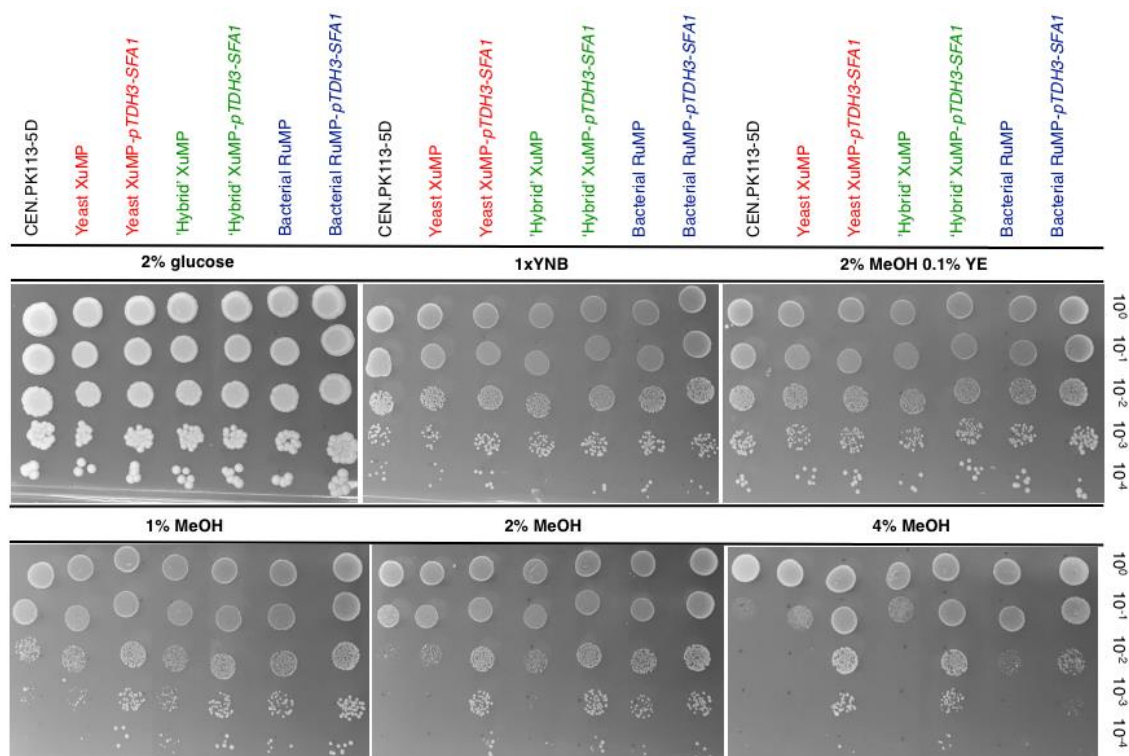
139

6

140

A

141
142

B

143

144 **Fig. 1. Methanol assimilation pathways engineered in *S. cerevisiae*. A.** Three different metabolic

145 pathways were engineered for methanol assimilation where methanol is oxidised to formaldehyde and later

146 assimilated to glyceraldehyde-3-phosphate or fructose-6-phosphate. The first yeast XuMP pathway (red) is targeted

147 to the peroxisome. The second 'hybrid' XuMP pathway (green) occurs in the cytosol. The third bacterial RuMP

148 pathway (blue) is also targeted to the cytosol and converts formaldehyde to fructose-6-phosphate. Over-expression of

7

149   the native formaldehyde detoxification enzyme Sfa1p is shown in bold. AOX1, alcohol oxidase 1; DAS1,

150   dihydroxyacetone synthase; PPP, pentose phosphate pathway; Mdh, methanol dehydrogenase; Hps, hexulose-6-

151   phosphate synthase; Phi, phospho-3-hexuloisomerase; SFA1, S-(hydroxymethyl) glutathione dehydrogenase; Xu5P,

152   xylulose-5-phosphate; Ru5P, ribulose-5-phosphate. **B.** Growth assays of different methanol assimilation pathways

153   with or without over-expression of the native formaldehyde detoxification pathway. Growth on increasing

154   concentrations of methanol was tested in serial 10-fold dilutions for an empty vector control, the yeast XuMP (red),

155   'hybrid' XuMP (green), or bacterial RuMP (blue) strain with or without over-expression of *SFA1*. Yeast Nitrogen

156   Base (YNB), Yeast Extract (YE), Methanol (MeOH). Images were taken after incubating at 30 ºC for 5 days.

157

158   **Enhancing native formaldehyde detoxification improves methanol-specific growth**

159   Methylotrophy is a delicate balance between formaldehyde assimilation and dissimilation.

160   Formaldehyde dissimilation to CO_2 is the main source of energy for methylotrophs, as the TCA

161   cycle is down-regulated when methanol is the sole carbon source [25]. While formaldehyde

162   assimilation *in S. cerevisiae* requires heterologous enzyme expression, a native pathway for the

163   dissimilation of formaldehyde to CO_2 and energy in the form of NADH already exists (Fig. 1A)

164   [26,27]. This pathway is initiated by an NAD_+ and glutathione-dependent formaldehyde

165   dehydrogenase, Sfa1p, which has previously been shown to enhance formaldehyde tolerance

166   when over-expressed in *S. cerevisiae* [28,29]. As formaldehyde accumulation in the cell can be

167   toxic, and its dissimilation plays an important role in methylotrophs, we chose to over-express

168   *SFA1* in *S. cerevisiae* alongside each of the three methanol assimilation pathways.

169

170   Growth of the yeast XuMP, 'hybrid' XuMP, or bacterial RuMP strains with or without over-

171   expression of *SFA1* was tested on solid minimal YNB medium with increased concentrations of

172   methanol or 2 % methanol with 0.1 % yeast extract, YNB medium with no added carbon source

173   (1 x YNB), or 2 % glucose (Fig. 1B). To confirm methanol assimilation, growth on methanol

174   would have to be visible independently of *SFA1* over-expression. For example, from Fig. 1B a

175   higher capacity for growth can be observed on 1 and 2 % methanol for the 'hybrid' XuMP and

176   bacterial RuMP strains. Enhanced formaldehyde dissimilation via *SFA1* over-expression had a

177   further positive effect on the growth of these strains at 2 % and 4 % methanol (Fig. 1B). This

178 distinct growth increase was most pronounced in the bacterial RuMP strain relative to both the

179 empty vector control strain on the same media, and relative to the same engineered strains on 1

180 x YNB medium. This experiment indicated three critical things: (i) the RuMP and 'hybrid'

181 pathways enabled methanol and formaldehyde assimilation in *S. cerevisiae*; (ii) the RuMP

182 pathway is superior to the 'hybrid' for formaldehyde assimilation; and (iii) *SFA1* over-

183 expression is an effective method for formaldehyde dissimilation, which is beneficial for growth

184 on methanol.

185

186 Further modifications aimed at improving growth on methanol of the 'hybrid' XuMP and

187 bacterial RuMP strains included targeting of *DAS1* to Ty1 sites for multiple genome insertion or

188 including the second enzymatically active dihydroxyacetone synthase (Das2p) in *P. pastoris* in

189 a new 'hybrid' XuMP *DAS1/DAS2* strain, as well as attempting to modulate flux through the

190 pentose phosphate pathway by over-expressing *TKL1* or *TAL1* in either strain (Supplementary

191 Fig. 1). Over-expression of these enzymes has been shown to improve pentose phosphate

192 pathway fluxes and availability of ribulose-5-phosphate [30-32]. Despite *TAL1* over-expression in

193 both strains enabling a slight growth increase when spotted onto solid minimal medium with 1,

194 2 or 4 % methanol (Supplementary Fig. 1), no growth increase was observed when tested in

195 liquid yeast extract methanol medium.

196

197 **Liquid growth and ^{13}C-methanol tracer analysis confirms methanol assimilation through**

198 **central carbon metabolism**

199 After observing methanol- and strain-specific growth differences on solid medium (Fig. 1B),

200 methanol-dependent growth of the 'hybrid' XuMP-*pTDH3-SFA1*, bacterial RuMP-*pTDH3-*

201 *SFA1*, and empty vector control strains was tested in liquid medium. No growth was observed

202 with 2 % methanol as the sole carbon source. Previous studies have highlighted the importance

203 of yeast extract for growth on liquid methanol media [33]. We therefore tested growth with and

204 without 2 % methanol in liquid YNB medium with 0.1 % yeast extract (Fig. 2A). The presence

205 of methanol in the medium resulted in significant ($p < 0.05$) final OD_{600} increases relative to

206   yeast-extract-only medium of 58 %, 47 %, and 39 % for the 'hybrid' XuMP-*pTDH3-SFA1*,

207   bacterial RuMP-*pTDH3-SFA1*, and control strains, respectively. This result identified a

208   methanol-specific growth increase in liquid medium containing yeast extract. In contrast to the

209   tests on solid methanol YNB medium (Fig. 1B), comparing the growth of the different strains

210   on liquid yeast extract methanol medium revealed only marginal and non-significant

211   differences. The presence of yeast extract appeared to largely eliminate the strain-specific

212   differences that were observed on solid YNB-methanol plates, which is consistent with the trend

213   observed on solid YNB-methanol plates with 0.1% yeast extract (Fig. 1B).

214

215   Due to the clear methanol response in all strains, and the marginal differences observed between

216   the wild-type and the engineered strains in liquid medium, the empty vector control strain

217   (CEN.PK 113-5D) was chosen for ^{13}C-methanol tracer analysis. Furthermore, as the effect of

218   methanol on the wild-type was unexpected, we first chose to verify methanol utilisation using

219   ^{13}C-tracer analysis in this strain. For ^{13}C-methanol tracer analysis, bioreactor off-gases such as

220   ^{13}C-methanol, ^{13}C-CO_2, CO_2, ^{13}C-ethanol, and ethanol were measured in real-time using a mass

221   spectrometer connected to the bioreactors. Intracellular metabolites were extracted and analysed

222   using Liquid Chromatography-Mass Spectrometry (LC-MS). When the ratio of labelled to

223   unlabelled CO_2 was compared at the maximum ^{13}C-CO_2 production point, 80 % of total CO_2

224   was produced as ^{13}C-CO_2 (Supplementary Fig. 2A). Surprisingly, CEN.PK 113-5D also

225   produced ^{13}C-ethanol (Fig. 2C), and ^{13}C-methanol tracer analysis furthered confirmed

226   assimilation with universally ^{13}C-labelled intracellular metabolites involved in the pentose

227   phosphate pathway, glycolysis, and the TCA cycle (Fig. 2B). Methanol assimilation through

228   central carbon metabolism was therefore identified in the wild-type strain with the detection of

229   various intracellular metabolites including ^{13}C-fructose 1,6-bisphosphate and ^{13}C-pyruvate,

230   which could only arise through the conversion of ^{13}C-methanol through central carbon

231   metabolism (Fig. 2B/C). This result showed for the first time that *S. cerevisiae* has a previously

232   undiscovered native capacity for methanol assimilation. The same ^{13}C-methanol tracer analysis

10

233 was performed for the bacterial RuMP-*pTDH3-SFA1* strain, which revealed a similar metabolic

234 profile as the one observed for CEN.PK 113-5D (Supplementary Fig. 2).
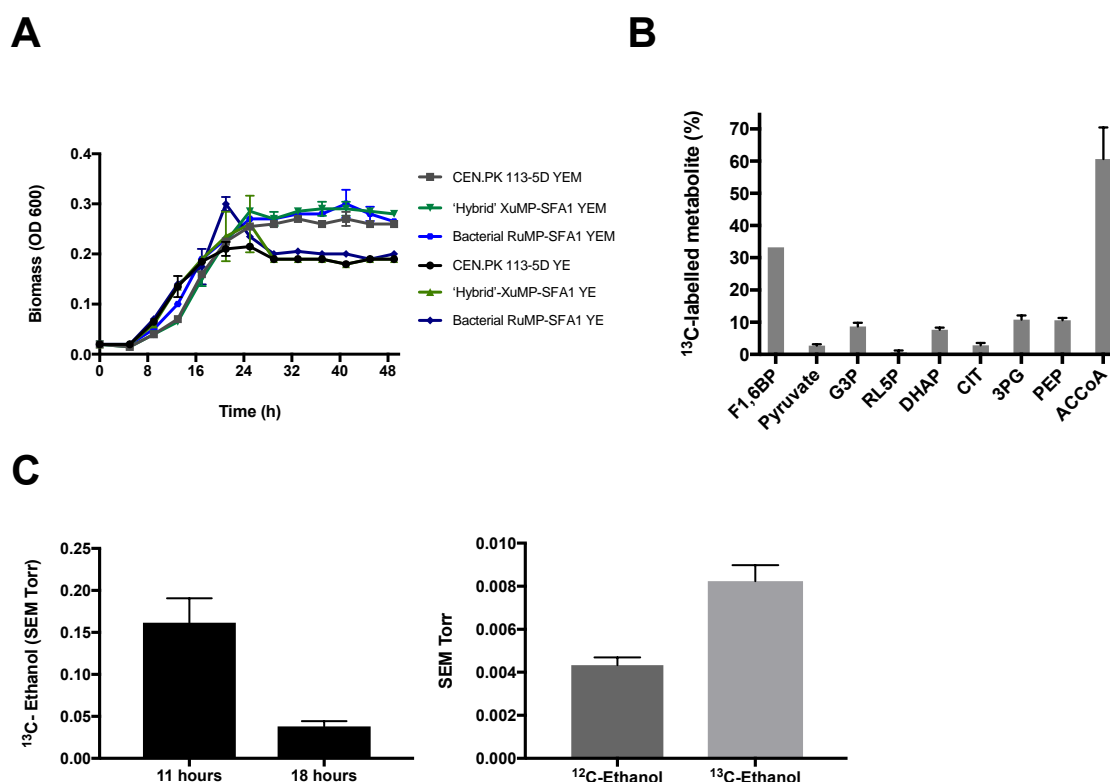
235

236
237

A

B

C

238

Fig. 2. ^{13}C-methanol fermentations confirm methanol assimilation in *S. cerevisiae*. A. Growth profiles
of CEN.PK 113-5D (the empty vector control), the 'hybrid' XuMP-*pTDH3-SFA1* and the bacterial RuMP-*pTDH3-*
SFA1 strain grown in liquid YNB medium with 0.1 % yeast extract (YE) or with 0.1 % yeast extract and 2 %
methanol (YEM). Data points represent the average of two biological replicates and error bars are the standard
deviation. **B.** Percentage of ^{13}C-labelled intracellular metabolites in CEN.PK 113-5D, metabolites are universally
(fully) labelled with ^{13}C. F1,6BP, fructose 1,6-bisphosphate; G3P, glyceraldehyde-3-phosphate; RL5P, ribulose-5-
phosphate; DHAP, dihydroxyacetone phosphate; CIT, citrate; 3PG, 3-phosphoglyceric acid; PEP,
phosphoenolpyruvate; ACCoA, acetyl-coenzyme A. Data points represent the average of two biological replicates
and error bars are the standard deviation. **C.** ^{13}C-ethanol was produced by CEN.PK 113-5D. The signal intensity was
normalised to the inert gas nitrogen, and then to biomass. Data shows the average ^{13}C-ethanol intensity at 47 amu for
two biological replicates during independent scanning cycles using a Hiden HPR-20-QIC mass spectrometer. Error
bars are the standard deviation of the ^{13}C-ethanol intensity. Ratio of ^{12}C-ethanol and ^{13}C-ethanol produced by
CEN.PK 113-5D at 18 hours. The signal intensity was normalised to the inert gas nitrogen, and then to biomass for

252 each strain. Data shows the average 12C-ethanol and 13C-ethanol intensity at 31 and 33 amu, respectively for two

253 biological replicates during independent scanning cycles using a Hiden HPR-20-QIC mass spectrometer. Error bars

254 are the standard deviation of the 12C-ethanol or 13C-ethanol intensity. SEM, Secondary Electron Multiplier (SEM);

255 amu, atomic mass unit.

256

257 **Adaptive laboratory evolution of native methanol assimilation in CEN.PK 113-5D**

258 As methanol assimilation in *S. cerevisiae* was previously undiscovered, Adaptive Laboratory

259 Evolution (ALE) was applied to characterise and optimise this metabolic response in the wild-

260 type CEN.PK 113-5D strain. The wild-type strain was selected for optimisation as only slight

261 differences in the metabolic profiles of the wild-type strain compared to the bacterial RuMP-

262 *pTDH3-SFA1* strain were observed. The ALE strategy consisted of three independent lineages

263 of CEN.PK 113-5D with an empty pRS416 vector grown with 1x YNB medium with either

264 yeast extract or yeast extract plus 2 % methanol. Yeast-extract-only medium was included to

265 track any improvements in fitness specific to yeast extract. Cultures were grown in baffled

266 shake flasks with alternating passages on 1 % glucose or yeast extract with or without methanol

267 (Fig. 3A). All six independent lineages were grown for 230 generations until a biomass (OD_{600})

268 increase in yeast extract methanol medium was observed. The six evolved strains were re-

269 sequenced to identify putative mutations leading to the phenotype. No relevant mutations were

270 observed in the three lineages evolved in yeast-extract-only medium. In contrast, the three

271 lineages evolved in yeast extract methanol medium all had point mutations at different positions

272 in *YGR067C*, an uncharacterised transcription factor with a DNA-binding domain similar to that

273 of *ADR1* (alcohol dehydrogenase II synthesis regulator). *ADR1* encodes a transcription factor

274 which is involved in the expression of glucose-repressed genes, ethanol metabolism, and

275 peroxisomal proliferation [34,35]. All three independent mutations resulted in premature stop

276 codons, which would result in truncation of the *YGR067C* protein (Fig. 3B). To test if

277 truncation of the *YGR067C* transcription factor was responsible for improved growth on

278 methanol, CRISPR-Cas9-mediated homologous recombination was used to introduce a stop-

279 codon in *YGR067C* of the wild-type strain as observed in the evolved lineage C (Fig. 3B). This

280   reconstructed CEN.PK 113-5D strain was referred to as reconstructed EC. The three evolved

281   lineages, the parental CEN.PK 113-5D, and reconstructed EC strains were grown on yeast

282   extract methanol medium to analyse growth differences (Fig. 3C). The evolved lineage A strain

283   had a final biomass increase of 37 % in the presence of methanol compared to the parental

284   CEN.PK 113-5D strain while the evolved lineage B and C strains have a 22 and 44 % increase

285   respectively. Importantly, the reconstructed EC strain has the same growth profile and final

286   biomass increase (44 %) as the evolved lineage C strain compared to the parental strain,

287   indicating that the truncated transcription factor is responsible for the beneficial response to

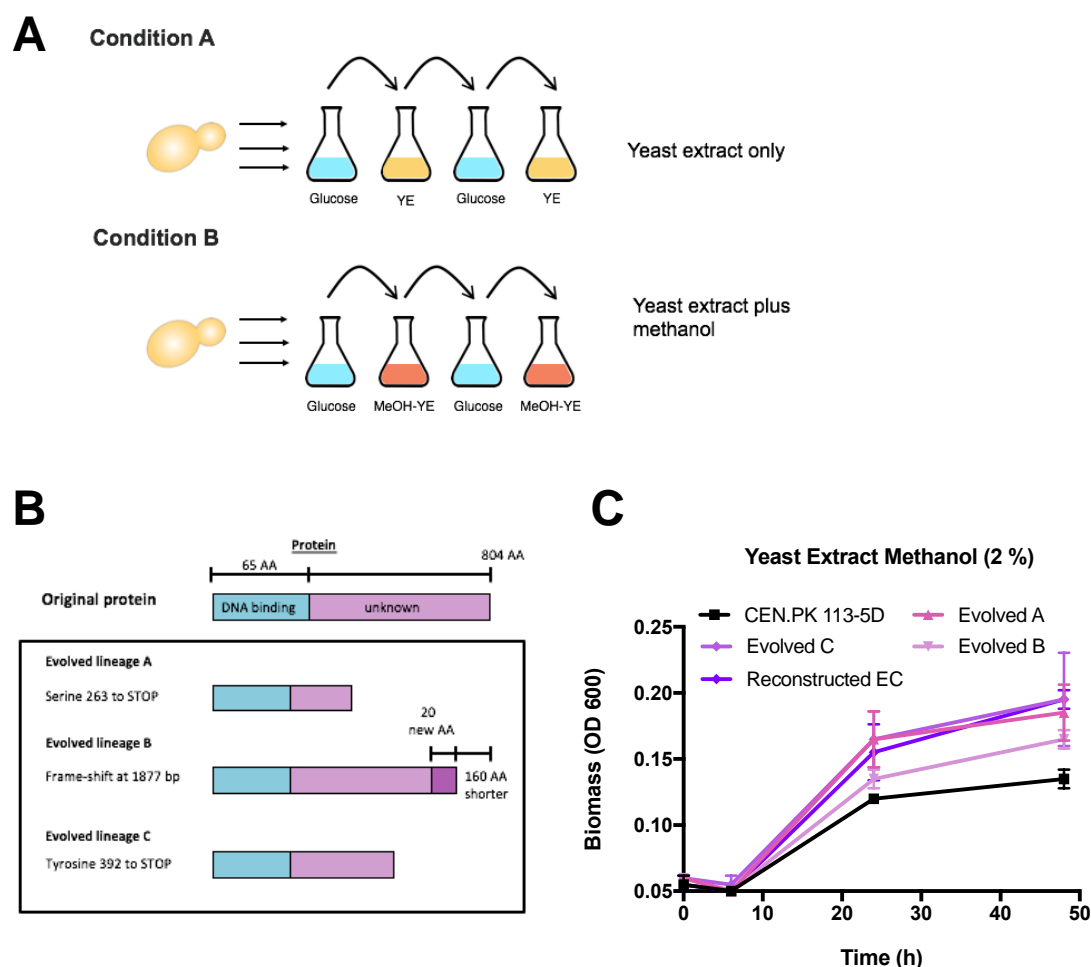288   methanol.

289

290

291   **Fig. 3. Adaptive Laboratory Evolution to improve native methanol assimilation in CEN.PK 113-**

292   **5D. A.** Schematic of the ALE design. Three independent lineages of CEN.PK 113-5D were grown in baffled shake

293   flasks in condition A or B for 230 generations. Under condition A, cultures were passaged from YNB medium

13

294 without amino acids and 1 % glucose (24 hours) to YNB medium without amino acids and 0.1 % yeast extract (48

295 hours). Under condition B, cultures were passaged from YNB medium without amino acids and 1 % glucose to YNB

296 medium without amino acids, 2 % methanol and 0.1 % yeast extract (48 hours). **B.** Schematic of the mutations in

297 *YGR067C* from the three evolved lineages grown under condition B, and the changes they caused to the protein, all

298 three mutations theoretically led to truncations. **C.** Growth profiles of CEN.PK 113-5D**,** the three evolved lineages in

299 condition B, and the reconstructed CEN.PK 113-5D strain with the mutation observed in the evolved lineage C.

300 Strains were grown in liquid YNB medium with 0.1 % yeast extract and 2 % methanol. Data points represent the

301 average of three biological replicates and error bars are the standard deviation.

302

303 **Reconstructed EC strain characterisation and ^{13}C-methanol tracer analysis**

304 To characterise the effect the reconstructed EC strain had on native methanol metabolism in *S.*

305 *cerevisiae*, CEN.PK 113-5D and the reconstructed EC strain were grown in bioreactors with 2

306 % ^{13}C-methanol and 0.1 % yeast extract. As previously noted (Fig. 3C), a growth advantage was

307 observed in the reconstructed EC strain (Fig. 4A), which reached a higher final biomass

308 compared to CEN.PK 113-5D. Both strains produced 80 % of total CO_2 as ^{13}C-CO_2 (Fig. 4B).

309 However, the reconstructed EC strain produced significantly less ^{13}C-ethanol, particularly at 11

310 hours (Fig. 4C). We hypothesized that the reconstructed EC strain could be redirecting

311 methanol into biomass constituents and thus reducing ethanol production. ^{13}C-methanol tracer

312 analysis revealed striking differences when intracellular metabolites were compared. The

313 reconstructed EC strain had a higher percentage of universally ^{13}C-labelled intracellular

314 metabolites compared to CEN.PK 113-5D (Fig. 5). A ~3-fold increase in ^{13}C-labelled

315 glyceraldehyde-3-phosphate and dihydroxyacetone phosphate was observed as well as increased

316 ^{13}C-labelling of metabolites involved in lower glycolysis, including 3-phosphoglyceric acid,

317 phosphoenolpyruvate, and pyruvate. ^{13}C-labelled pyruvate increased from 2.7 % in

318 CEN.PK113-5D to 15.4 % in the reconstructed EC strain. Higher ^{13}C-labelling was also

319 observed for metabolites in the pentose phosphate pathway but the proportion of ^{13}C-labelled

320 metabolites was still low in both strains (less than 5 %). An interesting observation was that

321 CEN.PK 113-5D had a higher proportion of ^{13}C-labelled acetyl-CoA compared to the

322   reconstructed EC strain, 67.6 % compared to 46.6 %. Finally, no unlabelled or $_{13}$C-labelled α-

323   ketoglutarate, fumarate, malate, oxaloacetate or glyoxylate were detected.

324

325   To further characterise the changes in the reconstructed EC strain, global transcript and protein

326   levels were compared with the parental strain (Fig. 5). During growth on 2 % $_{13}$C-methanol and

327   0.1 % yeast extract, 243 transcripts were found to be significantly differentially expressed in the

328   reconstructed EC strain (adjusted p < 0.01) with 111 genes down-regulated and 132 genes up-

329   regulated (Supplementary File 1). Gene-list analysis of the down-regulated genes showed Gene

330   Ontology (GO) pathway enrichment of the TCA cycle, respiration, and the glyoxylate cycle. No

331   pathway enrichment was found for the up-regulated genes in the reconstructed EC strain but GO

332   process enrichment was found for 'carbohydrate transmembrane transport', 'carbohydrate

333   metabolic process', 'glycolytic process' and 'pyruvate metabolic process', among others. The

334   proteomics analysis showed 103 proteins were significantly altered in abundance in the

335   reconstructed EC strain relative to the parent (adjusted p < 0.05; Supplementary File 2) with 84

336   proteins increased and 19 proteins decreased. Gene-list analysis of proteins with increased

337   expression showed pathway enrichment of the 'superpathway of glucose fermentation' while

338   the proteins with decreased abundance showed GO process enrichment only for 'trehalose

339   metabolic process'. When comparing the proteome of the reconstructed EC strain to that of the

340   parental CEN.PK 113-5D strain, 79 proteins were not identified in the proteome of the parental

341   strain, while 14 proteins were not identified in the reconstructed EC strain (Supplementary File

342   2).

343

344   Both transcriptomics and proteomics indicated there were significant changes in central carbon

345   metabolic pathway expression between the evolved and parental strain. Five genes involved in

346   glycolysis had higher transcript abundance in the reconstructed EC strain compared to CEN.PK

347   113-5D (*HXK1*, *GLK1*, *DAK2*, *TDH1* and *ENO2*) while *FBP1*, coding for fructose-1,6-

348   bisphosphatase, a key enzyme involved in gluconeogenesis [36,37], had lower transcript

349   abundance. Hxk1p, Glk1p, Tdh1p, and Eno2p also had increased protein abundance, as well as

15

350   Pfk1p, suggesting glycolysis rather than gluconeogenesis is predominantly occurring during

351   growth on methanol in the reconstructed EC strain. The increased transcript abundance of the 6-

352   phosphofructo-2-kinase glycolysis regulator *PFK27* [38] in the reconstructed EC strain also

353   supports this concept. Similar to the metabolite profile of the reconstructed EC strain, lower

354   transcript abundance was observed for nine genes involved in the TCA cycle (*CIT1, CIT2,*

355   *ACO1*, *IDH1*, *IDH2*, *KGD2*, *SDH1*, *SDH3* and *FUM3*; Fig. 5), suggesting the TCA cycle is

356   downregulated during growth on methanol. Sfa1p, which is involved in native formaldehyde

357   detoxification and alcohol oxidation also had increased protein abundance in the reconstructed

358   EC strain. This is consistent with the growth benefit we observed from *SFA1* over-expression

359   (Fig. 1B & Fig. 2A). Finally, the pentose phosphate pathway showed interesting results, with

360   *RKI1* having lower transcript abundance and Tkl2p lower protein abundance while Tal1p and

361   Fba1p had higher protein abundance. This could suggest transaldolase instead of transketolase

362   is the preferred enzyme to yield ribose-5-phosphates through the non-oxidative branch of the

363   pentose phosphate pathway in the reconstructed EC strain.

364

365   After characterising the reconstructed EC strain and identifying an improvement in native

366   methanol assimilation, the synthetic pathways highlighted in Fig. 1 were engineered into the

367   reconstructed EC strain (Supplementary Fig. 3). The synthetic pathways improved growth in the

368   reconstructed EC strain as they did in the parental CEN.PK 113-5D strain (Fig. 1B & 2A). The

369   'hybrid' XuMP and bacterial RuMP with over-expression of *SFA1* had increased growth on

370   solid minimal media with increasing concentrations of methanol compared to the reconstructed

371   EC strain (Supplementary Fig. 3A), however, no growth advantage was observed when the

372   reconstructed EC strain containing the bacterial RuMP-*pTDH3-SFA1* pathway was grown in

373   bioreactors with yeast extract and ^{13}C-methanol (2 %) medium (Supplementary Fig. 3B). The

374   presence of yeast extract results in slight, non-significant strain-specific differences, as was

375   previously observed when comparing growth on solid methanol media with liquid yeast extract

376   methanol media (Fig. 1B & Fig. 2A). Finally, both the reconstructed EC strain and the

377   reconstructed EC strain containing the bacterial RuMP-*pTDH3-SFA1* pathway show a similar

378   metabolic profile (Supplementary Fig. 3C/D/E) suggesting no meaningful differences are

379   apparent between the strains when grown in liquid medium, although significant methanol-
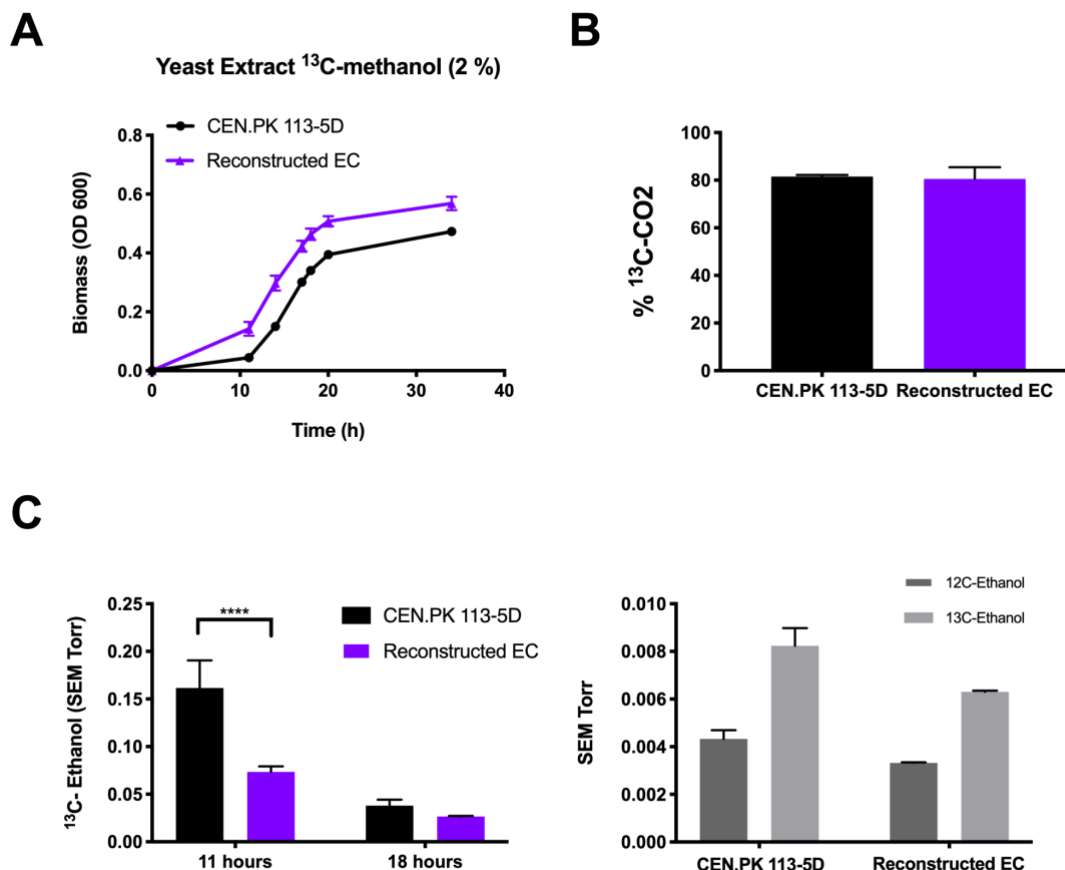
380   specific differences were apparent on solid medium.

381

382
383
384   **Fig. 4. ^{13}C-methanol fermentations to characterise the reconstructed evolved strain. A.** Growth

385   profile of CEN.PK 113-5D and the reconstructed evolved strain grown in liquid YNB medium with 2 % ^{13}C-

386   methanol supplemented with 0.1 % yeast extract cultures in bioreactors. **B.** Percentage of ^{13}C-CO_2/CO_2 production in

387   yeast extract ^{13}C-methanol (2 %) medium **C.** ^{13}C-ethanol was produced by CEN.PK 113-5D and by the reconstructed

388   evolved strain. The signal intensity was normalised to the inert gas nitrogen, and then to biomass for each strain. Data

389   shows the average ^{13}C-ethanol intensity at 47 amu for two biological replicates during independent scanning cycles

390   using a Hiden HPR-20-QIC mass spectrometer. Error bars are the standard deviation of the ^{13}C-ethanol intensity.

391   Ratio of ^{12}C-ethanol and ^{13}C-ethanol produced at 18 hours. The signal intensity was normalised to the inert gas

392   nitrogen, and then to biomass for each strain. Data shows the average ^{12}C-ethanol and ^{13}C-ethanol intensity at 31 and

393   33 amu, respectively for two biological replicates during independent scanning cycles using a Hiden HPR-20-QIC

394   mass spectrometer. Error bars are the standard deviation of the ^{12}C-ethanol or ^{13}C-ethanol intensity. SEM, Secondary

17

395   Electron Multiplier; amu, atomic mass unit. Data points represent the average of two biological replicates and error

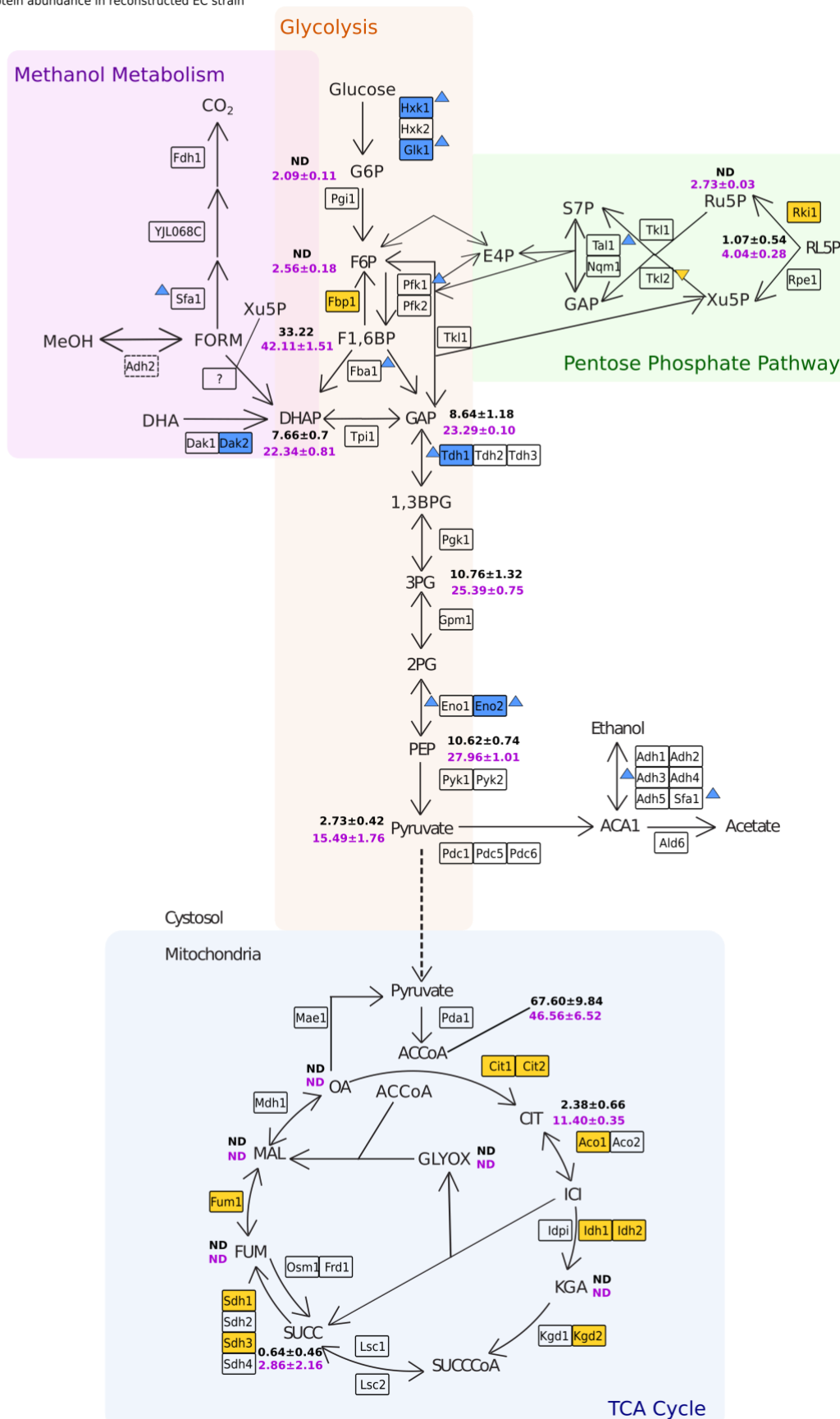396   bars are the standard deviation.

399 **Fig. 5. Characterisation of the reconstructed evolved strain at the metabolite, transcriptome and**

400 **proteome level compared to the parental strain during 13C-methanol fermentations.** Percentage of 13C-

401 labelled intracellular metabolites in CEN.PK 113-5D (black) and the reconstructed evolved strain (purple) at

402 exponential phase. Metabolites are universally (fully) labelled with 13C. Data points represent the average of two

403 biological replicates with standard deviation. Transcript and protein abundance in the reconstructed evolved strain

404 compared to the parental strain. Genes with up- or down-regulated fold-changes and adjusted p-values less than 0.01

405 are coloured blue or yellow respectively. Increased or decreased protein abundance and adjusted p-values less than

406 0.05 is shown in blue or yellow arrows respectively. RNA and protein samples were taken at stationary phase. ND;

407 not detected. The metabolic map was adapted from 39.

408

409 *ADH2* **and** *ACS1* **deletion reduces methanol-specific growth**

410 Eight genes were selected to analyse their potential role in native methanol assimilation in the

411 reconstructed EC strain. Firstly, the gene coding for an alcohol dehydrogenase 2 (*ADH2*) was

412 selected as in a separate study it was significantly up-regulated in response to methanol 40 and

413 due to the promiscuity of alcohol dehydrogenases in *S. cerevisiae*, it could be oxidising

414 methanol to formaldehyde. *CAT8*, coding for a transcription factor involved in de-repressing

415 genes during growth on non-fermentable carbon sources and thought to regulate the mutated

416 transcription factor Ygr067cp 41 (Fig. 3B) was chosen to analyse its effect on methanol growth.

417 The serine hydroxymethyltransferase gene (*SHM1*) was chosen for deletion as another

418 possibility for C1 carbon assimilation in *S. cerevisiae* involves formaldehyde detoxification to

419 formate and then assimilation through the glycine cleavage complex 42. Shm1p is responsible

420 for converting serine to glycine and 5,10-methylenetetrahydrofolate and would be required if

421 biomass formation was due to formaldehyde detoxification and subsequent formate

422 assimilation. The second set of genes selected for analysis were *DAK2*, *ENO1*, *ENO2, WSC3*,

423 and *ACS1*. *DAK2* and *ENO2*, coding for a dihydroxyacetone kinase and a phosphopyruvate

424 hydratase, respectively, were selected as they had higher transcript abundance in the

425 reconstructed EC strain compared to the parent and would be required for important steps

426 during glycolysis (Fig. 5). *ENO1* was also selected as it is a paralog of *ENO2* 43. *WSC3* was

427 selected as a putative methanol sensor since a study by Ohsawa et al. (2017) identified Wsc1p

428   and Wsc3p from *P. pastoris* as sensors involved in its native methanol response, with Wsc3p

429   from *P. pastoris* having 67.4 % amino acid sequence similarity with Wsc3p from *S. cerevisiae*

430   [44]. Wsc3p in *P. pastoris* is thought to act as a methanol sensor involved in activating a signalling

431   cascade for the expression of methanol-inducible genes. Finally, *ACS1* coding for an Acetyl-

432   CoA synthetase was selected as a study by Oshawa et al. (2018) analysed the role of *ACS1* in *P.*

433   *pastoris* and found that its involved in ethanol repression, which is needed for the expression of

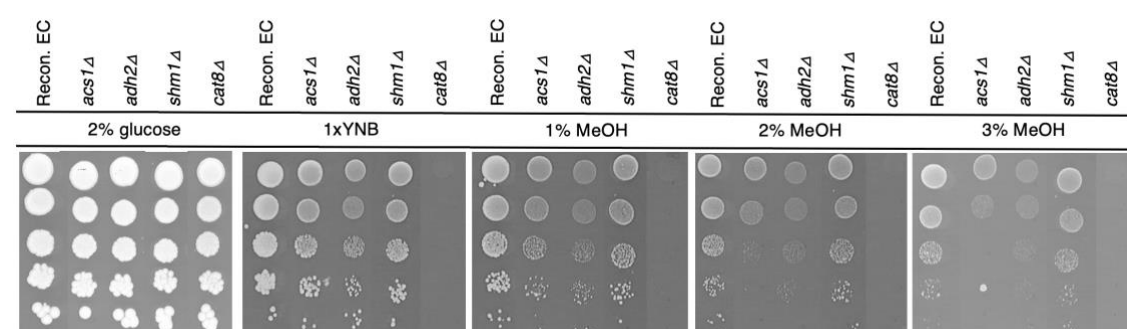434   methanol-induced genes [45].

435

437   **Fig. 6. Growth in methanol of different gene deletions to test their putative involvement *in S.***

438   ***cerevisiae*'s native methanol assimilation.** Growth on solid 1x Yeast Nitrogen Base medium with different

439   carbon sources was tested using serial 10-fold dilutions of the reconstructed evolved strain with an empty vector or

440   *ACS1, ADH2*, *SHM1* or *CAT8* deletions. Yeast Nitrogen Base (YNB), Yeast Extract (YE), Methanol (MeOH).

441   Images were taken after incubating at 30 ℃ for 6 days.

442

443   Single deletion strains of the aforementioned genes, except for *DAK2*, were constructed in the

444   reconstructed EC strain and tested by spotting the strains onto solid minimal YNB medium with

445   2 % glucose, no additional carbon source, or increasing methanol concentrations (Fig. 6 &

446   Supplementary Fig. 4). The reconstructed EC strain *Δadh2* grew similarly to the reconstructed

447   EC strain in minimal medium with 2 % glucose or no additional carbon source (1 x YNB) but

448   growth was dramatically reduced on media containing methanol (1 to 3 %), suggesting it is

449   needed for methanol oxidation to formaldehyde. When *Δcat8* was deleted from the

450   reconstructed EC strain, growth was only observed with 2 % glucose as the carbon source, and

451   its deletion dramatically decreased growth on methanol and 1 x YNB, as previously reported [46].

452   Any potential role of *CAT8* in methanol assimilation could therefore not be analysed using this

453   method. Deletion of *SHM1* had no effect on growth compared to the reconstructed EC strain on

454   media with either glucose or methanol, suggesting it is not involved in the native methanol

455   assimilation pathway. Finally, the reconstructed EC strains with *Δeno2, Δeno1, Δacs1, Δwsc3*

456   showed inconclusive results (Supplementary Fig. 4). The reconstructed EC strain with *Δeno2*

457   and *Δwsc3* had slight growth reductions on media with methanol but not glucose, *Δacs1* showed

458   almost no growth when methanol was present at higher concentrations (2 and 3 %), and *Δeno1*

459   showed no growth differences between media.

460

461   **Discussion**

462   As methanol is emerging as an important C1 feedstock, we engineered the XuMP and RuMP

463   methanol assimilation pathways in *S. cerevisiae* (Fig. 1A), and analysed growth on methanol as

464   well as ^{13}C-metabolite production from ^{13}C-methanol. The XuMP pathway was targeted either

465   to the peroxisome or to the cytosol, where a 'hybrid' version of the pathway was designed. A

466   subtle growth improvement only on solid 1 % methanol medium was observed when the

467   enzymes were targeted to the peroxisome by a PTS1 signal (Fig. 1B). This pathway is based on

468   *P. pastoris* metabolism, in which peroxisome proliferation plays a major role during growth on

469   methanol, a common characteristic of other methylotrophic yeasts [29,47]. However, peroxisome

470   proliferation in *S. cerevisiae* is limited to specific stress responses such as fatty acid oxidation

471   and requires the regulation of multiple genes [48]. It is possible that peroxisome proliferation was

472   a limiting step for the function of the XuMP pathway as peroxisome proliferation in response to

473   methanol has not evolved in *S. cerevisiae*. In conclusion, a XuMP methanol assimilation

474   pathway targeted to the peroxisome did not appear to be a viable option for synthetic

475   methylotrophy in *S. cerevisiae*. This contradicts a previous report by Dai et al. where up to 12 %

476   improvement on growth was recorded in yeast extract methanol (1 %) medium after

477   introduction of the yeast XuMP pathway (Aox1p-Das1p-Cat1p-Dak1p or Aox1p-Das2p-Cat1p-

478   Dak1p) [49].

479

480   The second, cytosol localised, 'hybrid' XuMP pathway utilised a bacterial NAD_+-dependent

481   Mdh alongside the *P. pastoris DAS1*. The third 'bacterial RuMP' pathway used enzymes from

482   methylotrophic bacteria (Mdh and Hps-Phi). An NAD_+-dependent methanol dehydrogenase was

483   chosen to oxidise methanol to formaldehyde (first step on the pathway), as it has been identified

484   as having higher affinity for methanol and the most efficient conversion compared to other

485   methanol dehydrogenases, especially the variant from *B. stearothermophilus* [16,18]. To assimilate

486   formaldehyde to biomass, enzymes utilising two different cyclic pathways were chosen, Das1p

487   (XuMP pathway) or Hps and Phi (RuMP pathway). These two alternatives were tested as they

488   use different co-substrates for formaldehyde assimilation (xylulose-5- phosphate or ribulose-5-

489   phosphate) and produce either glyceraldehyde-3-phosphate or fructose-6-phosphate as the

490   precursors for biomass formation (Fig. 1A). Both pathways enabled a greater capacity for

491   growth on solid minimal methanol medium relative to an empty vector control strain, with the

492   bacterial RuMP pathway being superior to the 'hybrid'-XuMP (Fig. 1B). This result is

493   supported by an *in silico* flux balance analysis performed by Comer et al., which analysed

494   different C1 carbon sources and also found the RuMP pathway to be the more promising option

495   in *S. cerevisiae* [50]. Moreover, a recent study in *Yarrowia lipolytica* containing an *FLD*

496   (formaldehyde dehydrogenase) deletion found that formaldehyde tolerance was recovered when

497   *B. methanolicus* Hps was introduced, while *P. pastoris* Das1p (with or without peroxisomal

498   targeting) was only capable of partially restoring formaldehyde tolerance [51].

499

500   An interesting development while testing the synthetic methylotrophic pathways in yeast was

501   the identification of formaldehyde detoxification as an important component of methanol-

502   dependent growth improvement. Studies on methylotrophic species have previously highlighted

503   the importance of the balance between assimilation and dissimilation of formaldehyde. Over-

504   expression of *SFA1*, the first gene in the native formaldehyde detoxification pathway, was

23

505 therefore tested alongside the three synthetic pathways. Growth on methanol was significantly

506 improved in all strains upon introduction of an over-expressed *SFA1* (Fig. 1B). Likewise,

507 methanol assimilation in solid minimal YNB-methanol media was identified in both the

508 'hybrid' XuMP and bacterial RuMP strains by comparing growth against an empty vector

509 control strain on increasing and toxic concentrations of methanol. Recent work has also

510 highlighted the importance of formaldehyde dissimilation through the engineering of synthetic

511 methylotrophy in *E. coli*. For example, Müller et al. detected an overall higher percentage of

512 total ^{13}C-labelling when they assessed methanol assimilation in a wild-type background

513 compared to a genetic background unable to dissimilate formaldehyde ($\Delta frmA$; 39.4 % versus

514 25.2 %), results that also contradicted their *in silico* simulations where formaldehyde

515 detoxification was not found to be essential for the conversion of methanol [16]. Woolston et al.

516 also investigated the improvement of formaldehyde assimilation in a synthetic methylotrophic

517 *E. coli* strain. They found that the unfavourable thermodynamics of the Mdh enzyme need to be

518 overcome to maintain the forward reaction direction of methanol oxidation [21]. One way to

519 achieve this is to maintain low intracellular formaldehyde levels through formaldehyde

520 dissimilation by over-expressing formaldehyde dehydrogenase. This observation could explain

521 why Müller et al. saw higher ^{13}C-labelling levels in a wild-type background that was able to

522 dissimilate formaldehyde, and together these observations support the importance of

523 formaldehyde dissimilation for methanol assimilation in *S. cerevisiae*.

524

525 Methanol-specific growth of the control, 'hybrid' XuMP-*pTDH3-SFA1* and bacterial RuMP-

526 *pTDH3-SFA1* strains, was observed in liquid yeast extract medium with methanol (Fig. 2A).

527 However, strain-specific differences in liquid yeast extract methanol medium were dramatically

528 diminished relative to those observed on minimal solid methanol medium, as observed when

529 yeast extract was added on solid medium (Fig. 1B). ^{13}C-labelled methanol was therefore used to

530 analyse the methanol response of CEN.PK 113-5D with an empty vector control in liquid

531 medium. Fermentations with 2 % ^{13}C-methanol were performed and quite surprisingly, ^{13}C-

532 ethanol and ^{13}C-labelled intracellular metabolites were produced (Fig. 2B/C), demonstrating

24

533   methanol assimilation through central carbon metabolism. Importantly, *S. cerevisiae* has always

534   been recognised as a non-native methylotroph and no previous growth on- or assimilation of-

535   methanol has been recorded in the literature. The identification of fully ^{13}C-labelled metabolites

536   from ^{13}C-methanol here clearly shows for the first time that methanol can be assimilated

537   through central carbon metabolism in *S. cerevisiae*.

538

539   After identifying native methanol assimilation in the wild-type, CEN.PK 113-5D strain, we

540   decided to focus on characterising and optimising this pathway. To optimise methanol

541   assimilation, an ALE strategy was designed where independent lineages of CEN.PK 113-5D

542   were passaged through conditional media (Fig. 3A). An evolutionary approach was chosen as

543   methanol assimilation in *S. cerevisiae* utilises an uncharacterised pathway and evolution can be

544   used to derive non-obvious solutions to complex and partially characterised systems.

545   Furthermore, laboratory evolution experiments have been successful in optimising consumption

546   of C1 carbon sources such as methanol and CO_2 in *E. coli*, and CO_2 in *P. pastoris* [15,52,53]. After

547   230 generations, growth was increased in liquid yeast extract methanol medium with whole-

548   genome sequencing revealing mutations in an uncharacterised putative transcription factor

549   *YGR067C* that lead to truncations of the protein (Fig. 3B). The mutation observed in the

550   evolved lineage C was reverse engineered into CEN.PK 113-5D, and the phenotype was

551   restored (Fig. 3C), confirming *YGR067C* is responsible for the optimised growth on methanol.

552   Little is known about Ygr067cp, it shares an identical DNA-binding domain with Adr1p and is

553   regulated by Cat8p [35,41]. Both Adr1p and Cat8p are involved in de-repressing genes needed for

554   growth on non-fermentable carbon sources [41], and Adr1p also activates genes involved in

555   peroxisomal biogenesis and proliferation [35]. Genes under the control of *ADR1* and relative to

556   methanol metabolism include formate dehydrogenases (*FDH1/FDH2*), *ADH2*, catalase (*CTA1*)

557   and *PEX11*, a peroxisomal membrane protein [35]. The truncation of Ygr067cp could have caused

558   the constant expression of genes that are normally repressed, leading to more favourable

559   regulatory conditions and metabolic fluxes for growth on methanol.

560

25

561   To characterise the improved growth on methanol, the reconstructed EC strain was grown in

562   bioreactors with 2 % ^{13}C-methanol and compared to the parental strain CEN.PK 113-5D (Fig.

563   4). The results confirmed the reconstructed EC strain had an improved capacity for methanol

564   assimilation, with higher proportions of ^{13}C-labelled intracellular metabolites observed (Fig. 5).

565   Moreover, integrated metabolomics, transcriptomics, and proteomics analyses showed that the

566   reconstructed EC strain has a different metabolic profile compared to the parent, with the TCA

567   cycle being downregulated as well as *FBP1*, an important regulator of gluconeogenesis (Fig. 5).

568   Together with the upregulated genes (*DAK2, TDH1* and *ENO2*) and higher protein abundance

569   of Pfk1p, Fba1p, Tdh1p, and Eno2p, it is likely that a net glycolytic flux is occurring during

570   methanol assimilation in the reconstructed EC strain.

571

572   Our results show that truncation of *YGR067C* causes decreased expression of gluconeogenesis,

573   TCA cycle, and glyoxylate cycle genes, which rearranges metabolic fluxes to favour methanol

574   assimilation. The down-regulated transcripts and proteins that we observed in the TCA and

575   glyoxylate cycles fully overlap with those that are normally de-repressed during growth on non-

576   fermentable carbon sources in a *CAT8* and *SNF1* dependent manner [35,41]. Given that *CAT8* is

577   known to regulate *YGR067C* [41], it is likely that truncation of the *YGR067C* protein facilitates a

578   decoupling of methanol assimilation from the traditional non-fermentable carbon source

579   utilisation phenotype in yeast. At present, it is unclear how these metabolic rearrangements

580   favour methylotrophy in *S. cerevisiae*. One possibility is that glycolytic rather than

581   gluconeogenic fluxes favour the pentose phosphate pathway fluxes necessary for methanol

582   assimilation in the presence of yeast extract. Another point worth noting is that many obligate

583   methylotrophs operate an incomplete, down-regulated TCA cycle through the absence of α-

584   ketoglutarate dehydrogenase activity, which is thought to preclude heterotrophic growth [54].

585

586   It is unclear how formaldehyde is assimilated in *S. cerevisiae*. However, the high levels of ^{13}C-

587   labelling we saw in dihydroxyacetone phosphate, fructose-1-6-bisphosphate, and

588   glyceraldehyde-3-phosphate suggests assimilation occurs via a mechanism similar to the *P.*

589   *pastoris* XuMP pathway where formaldehyde and xylulose-5-phosphate are converted into

590   dihydroxyacetone and glyceraldehyde-3-phosphate. From the higher transcript abundance of

591   Tal1p and Fba1p, an interesting idea worth exploring is whether the non-oxidative branch of the

592   pentose phosphate pathway is going through different rearrangement reactions than those when

593   *S. cerevisiae* is grown in glucose to recycle the co-substrates needed for formaldehyde

594   assimilation. Transaldolase could be catalysing the rearrangements of fructose-6-phosphate and

595   sedoheptulose-7-phosphate to glyceraldehyde-3-phosphate and erythrose-4-phosphate as it was

596   recently postulated in *P. pastoris* grown on methanol [25,55]. To identify specific genes involved in

597   native methanol assimilation, *ADH2* and six other genes were deleted from the reconstructed

598   EC strain. Another study from our group found that *ADH2* was upregulated when *S. cerevisiae*

599   was grown in the presence of methanol [40] and when the reconstructed EC strain with an *ADH2*

600   deletion was grown on solid minimal media with increasing concentrations of methanol, growth

601   was severely hindered in all cases, suggesting its role in oxidising methanol to formaldehyde

602   (Fig. 6). We also observed that deletion of acetyl-CoA synthetase (*ACS1*) reduced growth on

603   solid methanol media (Fig. 6). Acs1p is important for growth on non-fermentable carbon

604   sources [56], and its homolog is an important regulator of methylotrophic metabolism in *P.*

605   *pastoris* [45,57]. Acs1p is therefore likely to be an important source of acetyl-CoA in *S. cerevisiae*

606   methanol metabolism. The –omics profile of the reconstructed EC strain as well as the

607   identification of Adh2p as the likely first enzyme involved in the native methanol assimilation

608   of CEN.PK 113-5D suggest a *P. pastoris*-like pathway is occurring.

609

610   This multi-pathway comparison identified the bacterial RuMP-*pTDH3-SFA1* strain as the best

611   candidate for synthetic methanol assimilation in *S. cerevisiae*. Additionally, native methanol

612   assimilation was identified in *S. cerevisiae* for the first time and optimised through ALE,

613   providing the possibility of exploring the newly discovered native methanol metabolism.

614   Insights into this native methanol response have been elucidated such as methanol oxidation to

615   formaldehyde by Adh2p and altered central carbon metabolism enzyme expression levels. It is

616   possible that *S. cerevisiae* shares some of the characteristics of methylotrophic yeasts like *P.*

617   *pastoris* and is assimilating methanol through an incomplete version of this methylotrophic

618   pathway (Fig. 1A). Higher transcript abundance of *DAK2* alongside higher protein abundance of

619   Tal1p and Fba1p and high ^{13}C-labelling of dihydroxyacetone phosphate also support this

620   hypothesis. Higher biomass formation, a complete understanding of native methylotrophic

621   metabolism, and the elimination of the requirement for yeast extract in liquid methanol medium

622   are the most immediate challenges remaining for the implementation of growth with methanol

623   as the sole carbon source in *S. cerevisiae*. Higher biomass formation is likely limited by the

624   inefficient regeneration of pentose phosphate sugars, which is needed to increase the rate of

625   formaldehyde assimilation. After robust methylotrophy is established in *S. cerevisiae*, a plethora

626   of existing metabolite production pathways could potentially be coupled to a methanol

627   converting 'platform strain' using the state-of-the-art genetic tools and the deep physiological

628   characterization available in this model organism. Together, the results from this work represent

629   an exciting step towards using sustainable feedstocks during microbial fermentations for

630   conversion to chemicals, fuels, materials, pharmaceuticals, and foods, and provide the first

631   glimpse of an unexplored metabolic network.

28

632 **Methods**

633 **Strains and Plasmids**

634 *S. cerevisiae* plasmids and strains used in this study are shown in Tables 1 and 2, respectively.

635 The genes were codon-optimised for *S. cerevisiae* and synthesised by GenScript USA Inc. DNA

636 manipulation and propagation were performed using standard techniques [58]. All *S. cerevisiae*

637 transformations were carried out using the lithium acetate method [59]. *AOX1*, *DAS1*, *mdh*, *hps*

638 and *phi* genes were designed with flanking loxPsym sites to enable compatibility with the

639 synthetic yeast genome SCRaMbLE system, however, this system was not tested during this

640 study [60]. The synthetic genes were amplified using PCR and cloned into the pRS416 plasmid

641 digested with SmaI using the NEBuilder® HiFi DNA Assembly Master Mix. The *SFA1, TAL1*

642 and *TLK1* genes from *S. cerevisiae* were over-expressed by amplifying the gene and its native

643 terminator from genomic DNA, and cloned under the control of the *TDH3* promoter. These

644 over-expression constructs were cloned into the relevant pRS416 plasmids containing methanol

645 assimilation enzymes, the NEBuilder® HiFi DNA Assembly Master Mix was used for Gibson

646 Assembly [61]. All Gibson Assemblies were verified via PCR with M13 primers. For multiple site

647 integration of *DAS1*, the gene was cloned into the pBDK1 plasmid between the *PGK1* promoter

648 and terminator flanked by Ty1 delta sites, and transformed into yeast as described previously [62],

649 cells were plated on minimal media with 0.5 % glucose and toxic levels of formaldehyde (4

650 mM) and incubated at 30 °C. To delete *ADH2*, *CAT8*, *SHM1*, *ENO1*, *ENO2*, *WSC3*, *ACS1* and

651 *DAK2* from the reconstructed EC strain, primers amplifying the open reading frame flanked by

652 500 bp homology regions were designed and the constructs were amplified from the BY4741

653 knockout collection [63]. Amplified constructs were then transformed into the reconstructed EC

654 strain and plated on Yeast Extract Peptone Dextrose (YPD) with Geneticin (200 μg / mL;

655 Gibco™ 10131035). Independent colonies were screened via PCR using primers that annealed

656 200 bp outside of the PCR-generated homology region. Deletion of *DAK2* was never achieved

657 despite multiple attempts. All plasmid maps are available in Supplementary File 3.

658

Media and growth conditions

Escherichia coli DH5α cells were used for plasmid propagation/storage and grown in lysogeny

broth media (1 % tryptone, 0.5 % yeast extract, 1 % NaCl) with ampicillin.

The strains were precultured on Yeast Nitrogen Base (YNB) medium without amino acids and

with 5 g/L ammonium sulfate (Sigma-Aldrich Y0626) and 10 g/L glucose. Growth experiments

were performed on YNB medium with 1 or 2 % methanol supplemented with 1 g/L yeast

extract (Merck 103753). Optical density readings at 600 nm (OD_{600}) were used to track growth.

For spot assays, swabs from streaked agar plates were pre-cultured twice in 10 mL of 1 x YNB,

1% glucose in sterile 50 mL Falcon tubes. During the exponential phase of the final pre-culture,

cells were washed twice in 10 mL of sterile MilliQ water and serially diluted 10-fold up to 10^{-4},

prior to spotting 5 μl from each dilution onto the indicated agar plates. Plates were incubated at

30°C for 5 days. Spot assay photos are representative of many repeated experiments. For the

Adaptive Laboratory Evolution experiment, three independent lineages of CEN.PK 113-5D

with pRS416 where grown on baffled shake flasks with 50 mL YNB medium containing 1 g/L

yeast extract or 1 g/L yeast extract with 2 % methanol (48 hours) pulsing with YNB medium

with 1 % glucose (24 hours), and incubated at 30°C. OD_{600} measurements were taken before

every passage and the cultures were inoculated at a starting OD_{600} of 0.2 if grown on conditional

media or OD_{600} of 0.02 if grown on glucose medium.

DNA extraction and whole-genome sequencing of ALE lineages

Glycerol stocks of the six independent evolutionary lineages were inoculated into 10 mL of

YPD medium and grown overnight. Cells were pelleted and washed twice in 10 mL sterile

MilliQ water by centrifuging at 4000 x g for 2 mins. Genomic DNA was extracted from pellets

using the Yeast DNA Extraction Kit from ThermoFisher (catalog number 78870) according to

the instructions. Whole genome sequencing was performed at the Ramaciotti Centre for

Genomics using Nextera XT library preparation and NextSeq500 2 x 150 bp sequencing. A

minimum of 11 million reads were generated per sample with >95 % of reads having Q20

686   quality scores, except for methanol evolved lineage B, which had 80 % of reads with at least

687   Q20. An annotated CEN.PK113-7D reference genome was generated by transferring annotated

688   coding sequences with greater than 95 % homology from the S288C reference genome to

689   CEN.PK113-7D FASTA files using Geneious Pro version 11 [64]. Untrimmed reads were mapped

690   to the annotated CEN.PK113-7D reference genome using Geneious Pro. Each sample had

691   greater than 99 % of reads mapped to the reference with approximately 100-fold coverage. Non-

692   synonymous single nucleotide variants (SNV) within coding sequences were identified at a

693   minimum coverage of 10x, read-variant frequency of 0.9, maximum variant p-value of 10-5,

694   and a minimum strand-bias p value of 10_{-5} when exceeding 65% bias. SNVs were annotated

695   onto the consensus sequence of each strain and SNVs present in the methanol-exposed lineages

696   but absent in the yeast extract only lineages were identified as potentially causative mutations.

697

698   **Reconstruction of evolved lineage C mutation in *YGR067C***

699   The methanol-exposed evolutionary lineages had convergent but non-identical mutations in

700   *YGR067C,* which all encoded truncations in the protein through premature stop codons. These

701   mutations were substitution of C to G at nucleotide position 788, deletion of A at position 1877,

702   and substitution of C at position 1176 to G. The C1176G mutation from lineage C was chosen

703   for reverse engineering into the parental CEN.PK113-5D strain due to the proximity of the

704   mutation to a favourable crispr-Cas9 PAM site. The mutation was constructed using a

705   previously described approach whereby a single pRS423 plasmid encoding the Cas9 protein, the

706   guide RNA, and a hygromycin selection marker is PCR amplified using primers that encode a

707   new guide sequence in their 5' extensions, which also have 20 nt of homology to one another

708   [65,66]. This PCR product was co-transformed with mutated *YGR067C* DNA that was PCR

709   amplified from evolved lineage C genomic DNA, with transformants selected for hygromycin

710   resistance on YPD agar plates. Crude genomic DNA was extracted using the lithium acetate-

711   SDS method as previously described [67]. Transformants were screened by PCR amplifying and

712   Sanger sequencing the putatively mutated region of *YGR067C*. 1 out of 12 tested colonies had

713   the desired mutation using this method. This strain was subsequently referred to as

714   'reconstructed EC'.

715

716   **ambr® 250 Bioreactor Fermentations**

717   Strains were pre-cultured as above in sterile 50 mL Falcon tubes prior to inoculation at an OD_{600}

718   of 0.02 in ambr® 250 (Sartorius Stedim) microbial bioreactors with 140 mL of medium.

719   Dissolved oxygen was maintained at a minimum level of 20 % via automatic control of stirring

720   speed, air sparging, and O_2 sparging. pH was maintained at 5 via the automatic addition of 5 M

721   potassium hydroxide or 1 M phosphoric acid, and temperature was kept at 30 °C. Bioreactors

722   were sampled robotically at indicated time-points, with 1 mL samples stored at -20 °C prior to

723   measurement of growth using OD_{600}.

724

725   **^{13}C- Methanol Fermentations**

726   Growth experiments in YNB medium supplemented with yeast extract (1 g/L) and ^{13}C-methanol

727   (2 %; Sigma-Aldrich 277177) were carried out aerobically (sparging air) at 30°C, agitation of

728   300 RPM, and with a starting volume of 250 mL of medium using the Multifors 2 bioreactor

729   system (Infors AG). pH was maintained between 4.8 and 5.2 using 3M H_3PO_4. For pre-

730   culturing, biological replicates of each strain were grown in liquid YNB medium for

731   approximately 15 h. Cultures were then passaged into a second pre-culture and grown to mid-

732   exponential phase (OD_{600nm} between 1 and 3). A third pre-culture was also grown to mid-

733   exponential phase and washed twice with sterile water before inoculating the experimental

734   cultures at an OD_{600} of 0.02.

735

736   **RNA-extraction, sequencing and transcriptome analysis**

737   30 mL of culture was centrifuged at 4 ºC 17,000 x g for 10 min, with pellets resuspended in

738   RNA later (Sigma Aldrich R0901) and stored at -20 ºC prior to RNA extraction. Total RNA was

739   extracted as previously described [40]. Library preparation and sequencing was performed at the

740   Ramaciotti Centre for Genomics using a TruSeq Stranded mRNA-seq preparation kit and

741   NextSeq 500 2x75bp sequencing. 30 million reads were generated per sample with Q30 > 93 %

742   and Q20 > 95 %. Untrimmed reads were mapped to the S288C genome with read counting and

743   differential expression analysis carried out using Geneious Pro version 11 [68] as previously

744   described [40]. Approximately 72 million reads were generated per sample. Genes with p-values

745   less than 0.01 were considered differentially expressed. Lists of up and down-regulated genes

746   were analysed for GO term and pathway enrichment using YeastMine at the Saccharomyces

747   Genome Database (https://yeastmine.yeastgenome.org/yeastmine/bag.do). Significant

748   enrichment against the background whole-genome gene list was identified with p-values less

749   than 0.05 and Holm-Bonferroni correction for multiple comparisons. A list of all significant

750   genes that were differentially expressed can be found in Supplementary File 1.

751

752   **Analytical methods**

753   *Off-gas data analysis*

754   Real-time analysis of bioreactor culture off-gas was achieved using a Hiden HPR-20-QIC mass

755   spectrometer (Hiden Analytical) that was connected to the bioreactors. The Faraday Cup

756   detector was used to monitor the intensities of N, Ar, CO_2, ^{13}C-CO_2, ethanol, ^{13}C-ethanol, and

757   ^{13}C-methanol at 28, 40, 44, 45, 27, 47, and 30 atomic mass unit (amu), respectively. To increase

758   sensitivity and detect the presence of ^{13}C-ethanol from the off-gas data, the Secondary Electron

759   Multiplier (SEM) detector was used to scan any intensities from 15 to 50 amu, with 47 and 48

760   amu corresponding to ^{13}C-ethanol. N intensity (constant during fermentation as nitrogen was an

761   inert gas in our experiments) at 28 amu was used to normalise the intensity from ^{13}C-ethanol.

762   The SEM detector scanned the intensities during two to six independent cycles for each

763   bioreactor and at two different time points.

764

765   *Metabolomics*

766   To measure intracellular metabolites samples were taken at 11 hours during the ^{13}C- methanol

767   (2 %) fermentations, quenched in methanol and frozen at −80 °C. For extraction, the pellet was

768   resuspended in 2 mLs of 50 % acetonitrile and transferred to 2 mL microcentrifuge tubes with

769   0.1 mm diameter glass beads, every sample had two technical replicates. Samples were vortexed

770   for 30 s using a Precellys 24 tissue homogenizer (Bertin Instruments) at 30 °C. Three rounds of

771   vortexing were performed allowing the samples to cool completely between rounds. Samples

772   were centrifuged for 3 min at 5,000 x g and the supernatant was transferred to a clean

773   microcentrifuge tube and stored overnight at −80 °C. 2 mL of samples were freeze-dried

774   overnight, then resuspended in 100 μL of water with 10 uM of azidothymidine (AZT) as

775   internal standard, then transferred to HPLC glass inserts for analysis.

776   Metabolites were analysed using liquid chromatography tandem mass spectrometry (LC-

777   MS/MS) as adapted from [69-71]. In brief, analyses were performed using a Dionex Ultimate 3000

778   HPLC system coupled to an ABSciex 4000 QTRAP mass spectrometer. Liquid chromatography

779   was performed using a 50 min gradient, detailed in Supplementary Table 1, with 300 μL/min

780   flowrate, on a Phenomenex Gemini-NX C18 column (150 x 2 mm, 3 μm, 110 A), with a guard

781   column (SecurityGuard Gemini-NX C18, 4 x 2 mm), and column temperature of 55 °C. The

782   mobile phases used were: 7.5 mM aqueous tributylamine (Sigma-Aldrich) with pH adjusted to

783   4.95 (±0.05) using acetic acid (Labscan) for Solvent A, and acetonitrile (Merck) for Solvent B.

784   Samples were kept at 4 °C in the autosampler and 10 μL were injected for analyses. The HPLC

785   was controlled by Chromeleon 6.80 software (Dionex). Mass spectrometry was achieved using

786   a scheduled multiple reaction monitoring (sMRM) method on the negative ionisation mode.

787   Details of the compound-specific parameters used in the sMRM analysis are listed in

788   Supplementary Table 2. Other hardware parameter values include: ion spray voltage -4500 V,

789   ion source nebuliser (GS1), ion source auxiliary (GS2), curtain (CUR) and collision (CAD)

790   gases were 60, 60, 20 and medium (arbitrary units), respectively, using an in-house ultra-high

791   purity liquid nitrogen tank (BOC). The auxiliary gas temperature was kept at 350 °C. The mass

792   spectrometer was controlled by Analyst 1.6.3 software (AB Sciex). Amounts obtained for each

793   metabolite detected were based on standard curves from serial dilutions of analytical standards,

794   purchase from Sigma, where L1 = 200000, L2 = 100000, L3 = 50000, ... L20 = 0.38 nM. This

795   number of standard dilutions guaranteed that the standard curves consisted of at least five data

796   points. Standard mix and pooled samples were regularly injected along the run sequence for

797   quality control. Collected data were processed using MultiQuant 2.1 (AB Sciex).

798

799   *Protein extraction and Mass Spectrometry-based proteomics*

800   Protein samples were centrifuged at 4 °C 17,000 x g for 10 min, the supernatant was discarded

801   and the cell pellet was washed with 1.5 mL of Gibco™ Phosphate-buffered Saline (Life

802   Technologies). Cells were resuspended in lysis buffer (5 % SDS, 50 mM triethylammonium

803   bicarbonate, 100 mM DTT, pH 7.55) and transferred to a microcentrifuge tube containing 0.5

804   mm diameter glass beads. Cells were disrupted by using a Precellys 24 tissue homogenizer

805   (Bertin Instruments) for 8 rounds of vortexing (30 s vortex, 45 s rest) without cooling.

806   Microcentrifuge tubes were centrifuged for 10 min at 14,000 RPM and supernatant was

807   transferred to a clean microcentrifuge tube and stored at -20 ºC. Samples were digested with

808   trypsin following the S-trap™ minis (ProtiFi, LCC.) protocol. The digested peptide mixtures

809   were concentrated using Millipore® ZipTip C18 (Merck) eluting with 70 % acetonitrile.

810   Residual acetonitrile was removed by vacuum centrifugation and peptides resuspended in 5 %

811   acetonitrile, 0.1% formic acid (aqueous) before analysis. Peptides were analysed using a

812   ThermoFisher Scientific UltiMate 3000 RSLCnano UHPLC system. Each sample was initially

813   injected onto a ThermoFisher Acclaim PepMap C_{18} trap reversed-phase column (300 µm x 5

814   mm nano viper, 5 µm particle size) at a flow rate of 20 µL/min using 2 % acetonitrile (aqueous)

815   for 5 min with the solvent going to waste. The trap column was switched in-line with the

816   separation column (ThermoFisher EasySpray Pepmap RSLC C_{18}, 150 µm x 150 mm, 2 µm) and

817   the peptides were eluted using a flowrate of 1.0 µL/min using 0.1 % formic acid in water (buffer

818   A) and 80 % acetonitrile in buffer A (buffer B) as mobile phases for gradient elution. Peptide

819   elution employed a 4-30 % acetonitrile gradient for 40 min followed by 30-50 % acetonitrile for

820   10 min and 50-95 % acetonitrile for 1 min at 40 °C. The total elution time was 60 min including

821   a 95 % acetonitrile wash followed by re-equilibration. For each sample run, a volume of 2 µL

822   equating to approximately 1 µg of peptide material from protein digestion was injected.

823   The eluted peptides from the C18 column were introduced to the MS via a nano-ESI and

824   analysed using the Q-Exactive HF-X. The electrospray voltage was 1.8 kV in positive ion

825   mode, and the ion transfer tube temperature was 275 °C. Employing a top-40ddMS2 acquisition

826   method, full MS-scans were acquired in the Orbitrap mass analyser over the range m/z 350–

827   1400 with a mass resolution of 120,000 (at m/z 200). The AGC target value was set at

828   3.00E+06. The 40 most intense peaks with a charge state between 2 and 5 were fragmented in

829   the high energy collision dissociation (HCD) cell with a normalised collision energy (NCE) of

830   28. MSMS spectra were acquired in the Orbitrap mass analyser with a mass resolution of

831   15,000 at m/z 200. The AGC target value for MSMS was set to 1.0E+05 while the ion selection

832   threshold was set to 1E+03 counts. The maximum accumulation times were 60 min for full MS-

833   scans and MSMS. For all the experiments, the dynamic exclusion time was set to 25 s, and

834   undetermined charge state species were excluded from MSMS.

835   Raw files were processed using MaxQuant [72] version 1.6.10.43 with the integrated Andromeda

836   search engine [73] and the following search parameters: trypsin digestion with a maximum of 2

837   missed cleavages, carbamidomethyl (C) as a fixed modification and oxidation (M) and acetyl

838   (protein N-term) as variable modifications. The MS data was searched against the SGD protein

839   sequence database (6,630 entries downloaded November 2019). A peptide spectrum match

840   False Discovery Rate (FDR) of 0.01 and a protein FDR of 0.01 were used as protein

841   identification level cut-offs. Label-free quantification (LFQ) [74] was performed using MaxQuant

842   LFQ intensities. Protein quantification analysis of the LFQ results was performed using Perseus

843   [75] version 1.6.10.0. The data was first filtered to remove identified proteins classified as

844   'reverse', 'only identified by site' and 'potential contaminants'. The two corresponding

845   biological replicates for CEN.PK 113-5D or the reconstructed EC strain were loaded separately

846   and classified as replicates. Proteins that were not present in at least one of the two biological

847   replicates were removed to further trim the dataset. All LFQ values were log2 transformed, the

848   median intensity was subtracted to all intensities for all samples to normalise the distribution,

849 and missing values were imputed to 0. Lastly, a two-sided *t*-test was performed between

850 CEN.PK 113-5D and the reconstructed EC strain, and proteins with FDR adjusted p-values of

851 less than 0.05 were designated as differentially expressed. The log2FC for the significant

852 proteins was then calculated. A list of all significant proteins that were differentially expressed

853 can be found in Supplementary File 2.

854
855
856 **Table 1. Plasmids used in this study.**

Name	Details	Origin
pRS416	Yeast centromeric plasmid, URA3 marker	Euroscarf [76]
ScMOX3a-416	*pTDH3-AOX1-CYC1t-pTEF1-DAS1-PHO5t-pSSA1-PYC1-ADH1t*-pRS416	This study
ScMOX3a-SFA1-416	*pTDH3-AOX1-CYC1t-pTEF1-DAS1-PHO5t-pSSA1-PYC1-ADH1t- pTDH3-SFA1-SFA1t* -pRS416	This study
ScMOX3e-416	*pTEF1-DAS1-PHO5t-pTDH3-mdh-CYC1t* -pRS416	This study
ScMOX3e2-416	*pTEF1-DAS1-PHO5t-pTDH3-mdh-CYC1t-pTEF2-DAS2-ADH1t*-pRS416	This study
ScMOX3e-SFA1-416	*pTEF1-DAS1-PHO5t-pTDH3-mdh-CYC1t-pTDH3-SFA1-SFA1t* -pRS416	This study
ScMOX3e-TLK1-416	*pTEF1-TKL1-TKL1t-pTEF1-DAS1-PHO5t-pTDH3-mdh-CYC1t*-pRS416	This study
ScMOX3e-TAL1-416	*pSSA1-TAL1-TAL1t-pTEF1-DAS1-PHO5t-pTDH3-mdh-CYC1t*-pRS416	This study
ScMOX3g-416	*pTEF1-hps-ADH1t-pTEF2-phi-PHO5t-pTDH3-mdh-CYC1t*-pRS416	This study
ScMOX3g-SFA1-416	*pTEF1-hps-ADH1t-pTEF2-phi-PHO5t-pTDH3-mdh-CYC1t-pTDH3-SFA1-SFA1t*- pRS416	This study
ScMOX3g-TKL1-416	*pTEF1-TKL1-TKL1t-pTEF1-hps-ADH1t-pTEF2-phi-PHO5t-pTDH3-mdh-CYC1t* -pRS416	This study
ScMOX3g-TAL1-416	*pSSA1-TAL1-TAL1t-pTEF1-hps-ADH1t-pTEF2-phi-PHO5t-pTDH3-mdh-CYC1t* -pRS416	This study

857

858
859 **Table 2. *Saccharomyces cerevisiae* strains used in this study.**
860

Name	Genotype, plasmids	Notes	Origin
CEN.PK 113-5D	MATa; ura3-52	Haploid laboratory strain with uracil auxotrophy, mating type 'a'	Euroscarf [76]
CEN01	CEN.PK 113-5D, pRS416	Prototrophic strain with empty *URA3* vector	This study
CEN02	CEN.PK 113-5D, ScMOX3a-416	Strain expressing yeast (XuMP) methanol assimilation pathway	This study

CEN03	CEN.PK 113-5D, ScMOX3a-SFA1-416	Strain expressing yeast (XuMP) methanol assimilation pathway and over-expression of *SFA1*	This study
CEN04	CEN.PK 113-5D, ScMOX3e-416	Strain expressing 'hybrid' (XuMP) methanol assimilation pathway	This study
CEN05	CEN.PK 113-5D, ScMOX3g-416	Strain expressing bacterial (RuMP) methanol assimilation pathway	This study
CEN06	CEN.PK 113-5D, ScMOX3e-TKL1-416	Strain expressing 'hybrid' methanol assimilation pathway and over-expression of *TKL1*	This study
CEN07	CEN.PK 113-5D, ScMOX3e-TAL1-416	Strain expressing 'hybrid' methanol assimilation pathway and over-expression of *TAL1*	This study
CEN08	CEN.PK 113-5D, ScMOX3e2-416	Strain expressing second version of the 'hybrid' methanol assimilation pathway (*mdh-DAS1/DAS2*)	This study
CEN09	CEN.PK 113-5D, ScMOX3g-TKL1-416	Strain expressing bacterial (RuMP) methanol assimilation pathway and over-expression of *TKL1*	This study
CEN10	CEN.PK 113-5D, ScMOX3g-TAL1-416	Strain expressing bacterial (RuMP) methanol assimilation pathway and over-expression of *TAL1*	This study
MOX01	CEN.PK 113-5D, ScMOX3e-SFA1-416	Strain expressing 'hybrid' (XuMP) methanol assimilation pathway and over-expression of *SFA1*	This study
MOX02	CEN.PK 113-5D, ScMOX3g-SFA1-416	Strain expressing bacterial (RuMP) methanol assimilation pathway and over-expression of *SFA1*	This study
REC. EC	CEN.PK 113-5D with modified *YGR067C*$_{Y263*}$, pRS416	Strain expressing a truncated Ygr067cp where Tyrosine at position 263 is replaced with a stop codon	This study
REC. EC1	CEN.PK 113-5D with modified *YGR067C*$_{Y263*}$, ScMOX3e-416	Strain expressing a truncated Ygr067cp where Tyrosine at position 263 is replaced with a stop codon, and the 'hybrid' (XuMP) methanol assimilation pathway	This study
REC. EC2	CEN.PK 113-5D with modified *YGR067C*$_{Y263*}$, ScMOX3e-TKL1-416	Strain expressing a truncated Ygr067cp where Tyrosine at position 263 is replaced with a stop codon, and the 'hybrid' methanol assimilation pathway and over-expression of *TKL1*	This study
REC. EC3	CEN.PK 113-5D with modified *YGR067C*$_{Y263*}$, ScMOX3e-TAL1-416	Strain expressing a truncated Ygr067cp where Tyrosine at position 263 is replaced with a stop codon, and the 'hybrid' methanol assimilation pathway and over-expression of *TAL1*	This study
REC. EC4	CEN.PK 113-5D with modified *YGR067C*$_{Y263*}$, ScMOX3e-SFA1-416	Strain expressing a truncated Ygr067cp where Tyrosine at position 263 is replaced with a stop codon, and the 'hybrid' (XuMP) methanol assimilation pathway and over-expression of *SFA1*	This study
REC. EC5	CEN.PK 113-5D with modified *YGR067C*$_{Y263*}$, ScMOX3a-416	Strain expressing a truncated Ygr067cp where Tyrosine at position 263 is replaced with a stop codon, and the yeast (XuMP) methanol assimilation pathway	This study

REC. EC6	CEN.PK 113-5D with modified *YGR067C$_{Y263*}$*, ScMOX3a-SFA1-416	Strain expressing a truncated Ygr067cp where Tyrosine at position 263 is replaced with a stop codon, and the yeast (XuMP) methanol assimilation pathway and over-expression of *SFA1*	This study
REC. EC7	CEN.PK 113-5D with modified *YGR067C$_{Y263*}$*, ScMOX3g-SFA1-416	Strain expressing a truncated Ygr067cp where Tyrosine at position 263 is replaced with a stop codon, and the bacterial (RuMP) methanol assimilation pathway and over-expression of *SFA1*	This study
REC. EC *adh2Δ*	CEN.PK 113-5D with modified *YGR067C$_{Y263*}$*, pRS416	Strain expressing a truncated Ygr067cp where Tyrosine at position 263 is replaced with a stop codon, and Adh2p deletion	This study
REC. EC *shm1Δ*	CEN.PK 113-5D with modified *YGR067C$_{Y263*}$*, pRS416	Strain expressing a truncated Ygr067cp where Tyrosine at position 263 is replaced with a stop codon, and Shm1p deletion	This study
REC. EC *cat8Δ*	CEN.PK 113-5D with modified *YGR067C$_{Y263*}$*, pRS416	Strain expressing a truncated Ygr067cp where Tyrosine at position 263 is replaced with a stop codon, and Cat8p deletion	This study
REC. EC *eno1Δ*	CEN.PK 113-5D with modified *YGR067C$_{Y263*}$*, pRS416	Strain expressing a truncated Ygr067cp where Tyrosine at position 263 is replaced with a stop codon, and Eno1p deletion	This study
REC. EC *eno2Δ*	CEN.PK 113-5D with modified *YGR067C$_{Y263*}$*, pRS416	Strain expressing a truncated Ygr067cp where Tyrosine at position 263 is replaced with a stop codon, and Eno2p deletion	This study
REC. EC *acs1Δ*	CEN.PK 113-5D with modified *YGR067C$_{Y263*}$*, pRS416	Strain expressing a truncated Ygr067cp where Tyrosine at position 263 is replaced with a stop codon, and Acs1p deletion	This study
REC. EC *wsc3Δ*	CEN.PK 113-5D with modified *YGR067C$_{Y263*}$*, pRS416	Strain expressing a truncated Ygr067cp where Tyrosine at position 263 is replaced with a stop codon, and Wsc3p deletion	This study

861

References

862

863 1   Scarlat, N., Dallemand, J.-F., Monforti-Ferrario, F. & Nita, V. The role of biomass and

864   bioenergy in a future bioeconomy: Policies and facts. *Environmental Development* **15**,

865   3-34, doi:10.1016/j.envdev.2015.03.006 (2015).

866 2   Tsao, G. T. *Annual reports on fermentation processes*. (Elsevier Science, 2014).

867 3   Cotton, C. A. R., Claassens, N. J., Benito-Vaquerizo, S. & Bar-Even, A. Renewable

868   methanol and formate as microbial feedstocks. *Current Opinion in Biotechnology* **62**,

869   168-180, doi:https://doi.org/10.1016/j.copbio.2019.10.002 (2020).

870 4   Whitaker, W. B., Sandoval, N. R., Bennett, R. K., Fast, A. G. & Papoutsakis, E. T.

871   Synthetic methylotrophy: engineering the production of biofuels and chemicals based

872   on the biology of aerobic methanol utilization. *Current Opinion in Biotechnology* **33**,

873   165-175, doi:https://doi.org/10.1016/j.copbio.2015.01.007 (2015).

874 5   Bennett, R. K., Steinberg, L. M., Chen, W. & Papoutsakis, E. T. Engineering the

875   bioconversion of methane and methanol to fuels and chemicals in native and synthetic

876   methylotrophs. *Current Opinion in Biotechnology* **50**, 81-93,

877   doi:https://doi.org/10.1016/j.copbio.2017.11.010 (2018).

878 6   Goeppert, A., Czaun, M., Jones, J.-P., Surya Prakash, G. K. & Olah, G. A. Recycling of

879   carbon dioxide to methanol and derived products closing the loop. *Chem. Soc. Rev.* **43**,

880   7995-8048, doi:10.1039/c4cs00122b (2014).

881 7   Heux, S., Brautaset, T., A. Vorholt, J., Wendisch, V. F. & Charles Portais, J. in

882   *Methane Biocatalysis: Paving the Way to Sustainability*   Ch. Synthetic Methylotrophy:

883   Past, Present, and Future 133-151 (2018).

884 8   Whitaker, W. B., Sandoval, N. R., Bennett, R. K., Fast, A. G. & Papoutsakis, E. T.

885   Synthetic methylotrophy: engineering the production of biofuels and chemicals based

886   on the biology of aerobic methanol utilization. *Current opinion in biotechnology* **33**,

887   165-175, doi:10.1016/j.copbio.2015.01.007 (2015).

888   9   Yang, Y.-M. *et al.* Production of 3-hydroxypropionic acid in engineered

889   *Methylobacterium extorquens* AM1 and its reassimilation through a reductive route.

890   *Microbial cell factories* **16**, 179, doi:10.1186/s12934-017-0798-2 (2017).

891   10   Kurtzman, C. P. Biotechnological strains of *Komagataella* (*Pichia*) *pastoris* are

892   *Komagataella phaffii* as determined from multigene sequence analysis. *Journal of*

893   *Industrial Microbiology & Biotechnology* **36**, 1435, doi:10.1007/s10295-009-0638-4

894   (2009).

895   11   Gellissen, G. Heterologous protein production in methylotrophic yeasts. *Applied*

896   *microbiology and biotechnology* **54**, 741-750, doi:10.1007/s002530000464 (2000).

897   12   Araya-Garay, J. M. *et al.* Construction of a novel *Pichia pastoris* strain for production

898   of xanthophylls. *AMB Express* **2**, 24, doi:10.1186/2191-0855-2-24 (2012).

899   13   Siripong, W. *et al.* Metabolic engineering of *Pichia pastoris* for production of

900   isobutanol and isobutyl acetate. *Biotechnology for Biofuels* **11**, 1, doi:10.1186/s13068-

901   017-1003-x (2018).

902   14   He, H., Edlich-Muth, C., Lindner, S. N. & Bar-Even, A. Ribulose monophosphate shunt

903   provides nearly all biomass and energy required for growth of *E. coli*. *ACS Synthetic*

904   *Biology* **7**, 1601-1611, doi:10.1021/acssynbio.8b00093 (2018).

905   15   Meyer, F. *et al.* Methanol-essential growth of *Escherichia coli*. *Nature Communications*

906   **9**, 1508, doi:10.1038/s41467-018-03937-y (2018).

907   16   Müller, J. E. N. *et al.* Engineering *Escherichia coli* for methanol conversion. *Metabolic*

908   *Engineering* **28**, 190-201, doi:10.1016/j.ymben.2014.12.008 (2015).

909   17   Tuyishime, P. *et al.* Engineering *Corynebacterium glutamicum* for methanol-dependent

910   growth and glutamate production. *Metabolic Engineering* **49**, 220-231,

911   doi:10.1016/j.ymben.2018.07.011 (2018).

912   18   Whitaker, W. B. *et al.* Engineering the biological conversion of methanol to specialty

913   chemicals in *Escherichia coli*. *Metabolic Engineering* **39**, 49-59,

914   doi:10.1016/j.ymben.2016.10.015 (2017).

41

915   19   Witthoff, S., Mühlroth, A., Marienhagen, J. & Bott, M. C(1) metabolism in

916   *Corynebacterium glutamicum*: an endogenous pathway for oxidation of methanol to

917   carbon dioxide. *Applied and environmental microbiology* **79**, 6974-6983,

918   doi:10.1128/AEM.02705-13 (2013).

919   20   Witthoff, S. *et al.* Metabolic engineering of *Corynebacterium glutamicum* for methanol

920   metabolism. *Applied and environmental microbiology* **81**, 2215 (2015).

921   21   Woolston, B. M., King, J. R., Reiter, M., Van Hove, B. & Stephanopoulos, G.

922   Improving formaldehyde consumption drives methanol assimilation in engineered *E.

923   coli*. *Nature Communications* **9**, 2387, doi:10.1038/s41467-018-04795-4 (2018).

924   22   Brandāo, R. L. *et al.* Investigating acid stress response in different *Saccharomyces*

925   strains. *Journal of Mycology* **2014**, 9, doi:10.1155/2014/178274 (2014).

926   23   DeLoache, W. C., Russ, Z. N. & Dueber, J. E. Towards repurposing the yeast

927   peroxisome for compartmentalizing heterologous metabolic pathways. *Nature

928   Communications* **7**, 11152, doi:10.1038/ncomms11152 (2016).

929   24   Ostergaard, S., Olsson, L. & Nielsen, J. Metabolic Engineering of *Saccharomyces

930   cerevisiae*. *Microbiology and Molecular Biology Reviews* **64**, 34,

931   doi:10.1128/MMBR.64.1.34-50.2000 (2000).

932   25   Rußmayer, H. *et al.* Systems-level organization of yeast methylotrophic lifestyle. *BMC

933   Biology* **13**, 80, doi:10.1186/s12915-015-0186-5 (2015).

934   26   Achkor, H. *et al.* Enhanced formaldehyde detoxification by overexpression of

935   glutathione-dependent formaldehyde dehydrogenase from *Arabidopsis*. *Plant

936   Physiology* **132**, 2248 (2003).

937   27   Overkamp, K. M. *et al.* Functional analysis of structural genes for NAD(+)-dependent

938   formate dehydrogenase in *Saccharomyces cerevisiae*. *Yeast* **19**, 509-520,

939   doi:10.1002/yea.856 (2002).

940   28   Baerends, R. J. S. *et al.* Engineering and analysis of a *Saccharomyces cerevisiae* strain

941   that uses formaldehyde as an auxiliary substrate. *Applied and environmental

942   microbiology* **74**, 3182-3188, doi:10.1128/AEM.02858-07 (2008).

42

943   29   van der Klei, I. J., Harder, W. & Veenhuis, M. Methanol metabolism in a peroxisome-
944   deficient mutant of *Hansenula polymorpha*: a physiological study. *Archives of*
945   *microbiology* **156**, 15-23, doi:10.1007/BF00418181 (1991).

946   30   Becker, J. & Boles, E. A modified *Saccharomyces cerevisiae* strain that consumes L-
947   arabinose and produces ethanol. *Applied and environmental microbiology* **69**, 4144
948   (2003).

949   31   Kuyper, M. *et al.* Metabolic engineering of a xylose-isomerase-expressing
950   *Saccharomyces cerevisiae* strain for rapid anaerobic xylose fermentation. *FEMS yeast*
951   *research* **5**, 399-409, doi:10.1016/j.femsyr.2004.09.010 (2005).

952   32   Walfridsson, M., Hallborn, J., Penttilä, M., Keränen, S. & Hahn-Hägerdal, B. Xylose-
953   metabolizing *Saccharomyces cerevisiae* strains overexpressing the TKL1 and TAL1
954   genes encoding the pentose phosphate pathway enzymes transketolase and
955   transaldolase. *Applied and environmental microbiology* **61**, 4184-4190 (1995).

956   33   Gonzalez, J. E., Bennett, R. K., Papoutsakis, E. T. & Antoniewicz, M. R. Methanol
957   assimilation in *Escherichia coli* is improved by co-utilization of threonine and deletion
958   of leucine-responsive regulatory protein. *Metabolic Engineering* **45**, 67-74,
959   doi:10.1016/j.ymben.2017.11.015 (2018).

960   34   Böhm, S., Frishman, D. & Mewes, H. W. Variations of the C2H2 zinc finger motif in
961   the yeast genome and classification of yeast zinc finger proteins. *Nucleic acids research*
962   **25**, 2464-2469, doi:10.1093/nar/25.12.2464 (1997).

963   35   Young, E. T., Dombek, K. M., Tachibana, C. & Ideker, T. Multiple Pathways Are Co-
964   regulated by the Protein Kinase Snf1 and the Transcription Factors Adr1 and Cat8.
965   *Journal of Biological Chemistry* **278**, 26146-26158, doi:10.1074/jbc.M301981200
966   (2003).

967   36   Klein, C. J., Olsson, L. & Nielsen, J. Glucose control in Saccharomyces cerevisiae: the
968   role of Mig1 in metabolic functions. *Microbiology* **144 (Pt 1)**, 13-24,
969   doi:10.1099/00221287-144-1-13 (1998).

37   Mercado, J. J. & Gancedo, J. M. Regulatory regions in the yeast *FBP1* and *PCK1* genes. *FEBS letters* **311**, 110-114, doi:10.1016/0014-5793(92)81379-Z (1992).

38   Rider, Mark H. *et al.* 6-Phosphofructo-2-kinase/fructose-2,6-bisphosphatase: head-to-head with a bifunctional enzyme that controls glycolysis. *Biochemical Journal* **381**, 561-579, doi:10.1042/BJ20040752 (2004).

39   Williams, T. C., Peng, B., Vickers, C. E. & Nielsen, L. K. The *Saccharomyces cerevisiae* pheromone-response is a metabolically active stationary phase for bio-production. *Metabolic Engineering Communications* **3**, 142-152, doi:10.1016/j.meteno.2016.05.001 (2016).

40   Espinosa, M. I., Williams, T. C., Pretorius, I. S. & Paulsen, I. T. Benchmarking two *Saccharomyces cerevisiae* laboratory strains for growth and transcriptional response to methanol. *Synthetic and Systems Biotechnology* **4**, 180-188, doi:10.1016/j.synbio.2019.10.001 (2019).

41   Haurie, V. *et al.* The transcriptional activator Cat8p provides a major contribution to the reprogramming of carbon metabolism during the diauxic shift in *Saccharomyces cerevisiae*. *The Journal of biological chemistry* **276**, 76-85, doi:10.1074/jbc.M008752200 (2001).

42   Gonzalez de la Cruz, J., Machens, F., Messerschmidt, K. & Bar-Even, A. Core catalysis of the reductive glycine pathway demonstrated in yeast. *ACS Synthetic Biology* **8**, 911-917, doi:10.1021/acssynbio.8b00464 (2019).

43   Byrne, K. P. & Wolfe, K. H. The Yeast Gene Order Browser: combining curated homology and syntenic context reveals gene fate in polyploid species. *Genome research* **15**, 1456-1461 (2005).

44   Ohsawa, S., Yurimoto, H. & Sakai, Y. Novel function of Wsc proteins as a methanol-sensing machinery in the yeast *Pichia pastoris*. *Molecular Microbiology* **104**, 349-363, doi:10.1111/mmi.13631 (2017).

45   Ohsawa, S., Nishida, S., Oku, M., Sakai, Y. & Yurimoto, H. Ethanol represses the expression of methanol-inducible genes via acetyl-CoA synthesis in the yeast

998   Komagataella phaffii. *Scientific Reports* **8**, 18051, doi:10.1038/s41598-018-36732-2

999   (2018).

1000   46   Gasmi, N. *et al.* The switch from fermentation to respiration in *Saccharomyces*

1001   *cerevisiae* is regulated by the Ert1 transcriptional activator/repressor. *Genetics* **198**, 547,

1002   doi:10.1534/genetics.114.168609 (2014).

1003   47   Veenhuis, M. & Harder, W. in *Peroxisomes in Biology and Medicine.* (eds H. Dariush

1004   Fahimi & Helmut Sies) 436-458 (Springer Berlin Heidelberg).

1005   48   Hiltunen, J. K. *et al.* The biochemistry of peroxisomal β-oxidation in the yeast

1006   *Saccharomyces cerevisiae*. *FEMS Microbiology Reviews* **27**, 35-64, doi:10.1016/S0168-

1007   6445(03)00017-2 (2003).

1008   49   Dai, Z. *et al.* Metabolic construction strategies for direct methanol utilization in

1009   *Saccharomyces cerevisiae*. *Bioresource Technology* **245**, 1407-1412,

1010   doi:10.1016/j.biortech.2017.05.100 (2017).

1011   50   Comer, A. D., Long, M. R., Reed, J. L. & Pfleger, B. F. Flux balance analysis indicates

1012   that methane is the lowest cost feedstock for microbial cell factories. *Metabolic*

1013   *Engineering Communications* **5**, 26-33, doi:10.1016/j.meteno.2017.07.002 (2017).

1014   51   Vartiainen, E. *et al.* Evaluation of synthetic formaldehyde and methanol assimilation

1015   pathways in *Yarrowia lipolytica*. *Fungal Biology and Biotechnology* **6**, 27,

1016   doi:10.1186/s40694-019-0090-9 (2019).

1017   52   Gassler, T. *et al.* The industrial yeast *Pichia pastoris* is converted from a heterotroph

1018   into an autotroph capable of growth on CO2. *Nature Biotechnology*,

1019   doi:10.1038/s41587-019-0363-0 (2019).

1020   53   Gleizer, S. *et al.* Conversion of *Escherichia coli* to generate all biomass carbon from

1021   CO2. *Cell* **179**, 1255-1263.e1212, doi:10.1016/j.cell.2019.11.009 (2019).

1022   54   Wood, A. P., Aurikko, J. P. & Kelly, D. P. A challenge for 21st century molecular

1023   biology and biochemistry: what are the causes of obligate autotrophy and

1024   methanotrophy? *FEMS Microbiology Reviews* **28**, 335-352,

1025   doi:10.1016/j.femsre.2003.12.001 (2004).

55   Stincone, A. *et al.* The return of metabolism: biochemistry and physiology of the pentose phosphate pathway. *Biol Rev Camb Philos Soc* **90**, 927-963, doi:10.1111/brv.12140 (2015).

56   Kratzer, S. & Schüller, H.-J. Carbon source-dependent regulation of the acetyl-coenzyme A synthetase-encoding gene ACSI from saccharomyces cerevisiae. *Gene* **161**, 75-79, doi:https://doi.org/10.1016/0378-1119(95)00289-I (1995).

57   Sahu, U. & Rangarajan, P. N. Regulation of Acetate Metabolism and Acetyl Co-a Synthetase 1 (ACS1) Expression by Methanol Expression Regulator 1 (Mxr1p) in the Methylotrophic Yeast Pichia pastoris. *J Biol Chem* **291**, 3648-3657, doi:10.1074/jbc.M115.673640 (2016).

58   Sambrook, J. & Russell, D. W. *Molecular cloning, a laboratory manual.* (Cold Spring Harbour Laboratory Press, 2001).

59   Gietz, R. D. & Schiestl, R. H. Quick and easy yeast transformation using the LiAc/SS carrier DNA/PEG method. *Nature protocols* **2**, 35, doi:10.1038/nprot.2007.14 (2007).

60   Dymond, J. & Boeke, J. The *Saccharomyces cerevisiae* SCRaMbLE system and genome minimization. *Bioengineered Bugs* **3**, 168-171, doi:10.4161/bbug.19543 (2012).

61   Gibson, D. G. *et al.* Enzymatic assembly of DNA molecules up to several hundred kilobases. *Nature Methods* **6**, 343, doi:10.1038/nmeth.1318 (2009).

62   Kroukamp, H., den Haan, R., van Wyk, N. & van Zyl, W. H. Overexpression of native PSE1 and SOD1 in S*accharomyces cerevisiae* improved heterologous cellulase secretion. *Applied Energy* **102**, 150-156, doi:10.1016/j.apenergy.2012.05.062 (2013).

63   Baker Brachmann, C. *et al.* Designer deletion strains derived from *Saccharomyces cerevisiae* S288C: A useful set of strains and plasmids for PCR-mediated gene disruption and other applications. *Yeast* **14**, 115-132, doi:10.1002/(SICI)1097-0061(19980130)14:2<115::AID-YEA204>3.0.CO;2-2 (1998).

1052   64   Kearse, M. *et al.* Geneious Basic: An integrated and extendable desktop software
1053   platform for the organization and analysis of sequence data. *Bioinformatics* **28**, 1647-
1054   1649, doi:10.1093/bioinformatics/bts199 (2012).

1055   65   Williams, T. C., Xu, X., Ostrowski, M., Pretorius, I. S. & Paulsen, I. T. Positive-
1056   feedback, ratiometric biosensor expression improves high-throughput metabolite-
1057   producer screening efficiency in yeast. *Synthetic Biology* **2**, doi:10.1093/synbio/ysw002
1058   (2017).

1059   66   Xu, X., Williams, T. C., Divne, C., Pretorius, I. S. & Paulsen, I. T. Evolutionary
1060   engineering in *Saccharomyces cerevisiae* reveals a *TRK1*-dependent potassium influx
1061   mechanism for propionic acid tolerance. *Biotechnology for Biofuels* **12**, 97,
1062   doi:10.1186/s13068-019-1427-6 (2019).

1063   67   Lõoke, M., Kristjuhan, K. & Kristjuhan, A. Extraction of genomic DNA from yeasts for
1064   PCR-based applications. *BioTechniques* **50**, 325-328, doi:10.2144/000113672 (2011).

1065   68   Kearse, M. *et al.* Geneious Basic: an integrated and extendable desktop software
1066   platform for the organization and analysis of sequence data. *Bioinformatics* **28**, 1647-
1067   1649, doi:10.1093/bioinformatics/bts199 (2012).

1068   69   Dietmair, S. *et al.* A multi-omics analysis of recombinant protein production in Hek293
1069   Cells. *PloS one* **7**, e43394, doi:10.1371/journal.pone.0043394 (2012).

1070   70   McDonald, T. S., Carrasco-Pozo, C., Hodson, M. P. & Borges, K. Alterations in
1071   cytosolic and mitochondrial [U-13C] glucose metabolism in a chronic epilepsy mouse
1072   model. *eneuro* **4**, ENEURO.0341-0316.2017, doi:10.1523/ENEURO.0341-16.2017
1073   (2017).

1074   71   Medina-Torres, C. E., van Eps, A. W., Nielsen, L. K. & Hodson, M. P. A liquid
1075   chromatography–tandem mass spectrometry-based investigation of the lamellar
1076   interstitial metabolome in healthy horses and during experimental laminitis induction.
1077   *The Veterinary Journal* **206**, 161-169, doi:10.1016/j.tvjl.2015.07.031 (2015).

1078   72   Cox, J. & Mann, M. MaxQuant enables high peptide identification rates, individualized

1079   p.p.b.-range mass accuracies and proteome-wide protein quantification. *Nature*

1080   *Biotechnology* **26**, 1367-1372, doi:10.1038/nbt.1511 (2008).

1081   73   Cox, J. *et al.* Andromeda: a peptide search engine integrated into the MaxQuant

1082   environment. *Journal of Proteome Research* **10**, 1794-1805, doi:10.1021/pr101065j

1083   (2011).

1084   74   Cox, J. *et al.* Accurate proteome-wide label-free quantification by delayed

1085   normalization and maximal peptide ratio extraction, termed MaxLFQ. *Mol Cell*

1086   *Proteomics* **13**, 2513-2526, doi:10.1074/mcp.M113.031591 (2014).

1087   75   Tyanova, S. *et al.* The Perseus computational platform for comprehensive analysis of

1088   (prote)omics data. *Nature Methods* **13**, 731-740, doi:10.1038/nmeth.3901 (2016).

1089   76   Sikorski, R. S. & Hieter, P. A system of shuttle vectors and yeast host strains designed

1090   for efficient manipulation of DNA in *Saccharomyces cerevisiae*. *Genetics* **122**, 19

1091   (1989).

1092

Acknowledgements

Author contributions

M.I.E and T.C.W conceived the study and designed the experiments. M.I.E performed the experiments, with contributions from T.C.W. M.I.E and T.C.W analysed data. M.I.E, E.M, K.V and R.A.G.G designed and performed the ^{13}C-labelling and bioreactor experiments. M.P designed the method to detect intracellular ^{13}C-labelled metabolites. C.S, T.C.W, I.S.P and I.T.P participated in the design, support, and coordination of the project. All authors read and approved the final manuscript.

Competing interests

None

Materials and correspondence

Thomas C. Williams: tom.williams@mq.edu.au, Ian T. Paulsen: ian.paulsen@mq.edu.au